HHS Public Access

Author manuscript

Cell Rep. Author manuscript; available in PMC 2026 March 20.

Published in final edited form as:

Cell Rep. 2026 February 24; 45(2): 116868. doi:10.1016/j.celrep.2025.116868.

Decoding the heterogeneity of human undifferentiated spermatogonia reveals RAS-dependent regulation of stem cell fate

Chiara Capponi[1], **Christopher Smith**[1], **Alexa Medica**[1], **Tung-Chin Hsieh**[2], **Kyle E. Orwig**[3], **Kun Tan**[1,4,*]

[1]Department of Obstetrics, Gynecology, and Reproductive Sciences, University of California San Diego, La Jolla, CA 92093, USA

[2]Department of Urology, University of California San Diego, La Jolla, CA 92103, USA

[3]Obstetrics, Gynecology and Reproductive Sciences, University of Pittsburgh School of Medicine, Magee-Womens Research Institute, Pittsburgh, PA 15213, USA

[4]Lead contact

SUMMARY

Spermatogonial stem cells (SSCs) are essential for long-term spermatogenesis and hold therapeutic potential for treating male infertility. While rodent SSCs are well characterized, human SSCs remain poorly understood. Here, we screen antibodies against proteins encoded by genes enriched in specific subsets of human undifferentiated spermatogonia (uSPG) identified by single-cell RNA sequencing. We characterize four markers labeling distinct uSPG subsets: PIWIL4 marks primitive, quiescent uSPG; EGR4 marks uSPG at a proliferative crossroads; and PPP1R36 and NANOS3 label distinct proliferative subsets poised for differentiation. The most and least advanced subsets—PIWIL4+ and NANOS3+ cells—do not overlap. Comparative transcriptomics uncover candidate pathways involved in uSPG fate transitions, including RAS signaling. Using

*Correspondence: kutan@health.ucsd.edu.

AUTHOR CONTRIBUTIONS

K.T. supervised and conceived this study. C.C. and K.T. designed the experiments. C.C., C.S., A.M., and K.T. conducted the experiments. T.-C.H. and K.E.O. provided the human testes samples. C.C. and K.T. wrote and edited the manuscript.

RESOURCE AVAILABILITY

Lead contact

Further information and requests for resources and reagents should be directed to and will be fulfilled by the lead contact, Dr. Kun Tan (kutan@ health.ucsd.edu).

Materials availability

This study did not generate new unique reagents. All the materials used in this study are preserved by Dr. Kun Tan's laboratory and are available upon request.

Data and code availability

RNA-seq data generated in this study have been deposited at NCBI's GEO database under the accession number GEO: GSE297876. No unpublished custom code, software, or algorithm was used in this study. Freely available software and algorithms used for analysis are listed in the key resources table. Any additional information required to reanalyze the data reported in this paper is available upon request from the lead contact, Kun Tan (kutan@health.ucsd.edu).

DECLARATION OF INTERESTS

K.E.O. is an advisor and co-founder of Paterna Biosciences. The work presented in this manuscript is not related to any Paterna Biosciences programs.

FSD1, a pan-uSPG cell-surface marker identified here, we purify the entire uSPG population and demonstrate that RAS signaling maintains the primitive uSPG state. These findings provide a framework for human uSPG identity, with broad implications for reproductive biology and regenerative medicine.

Graphical Abstract

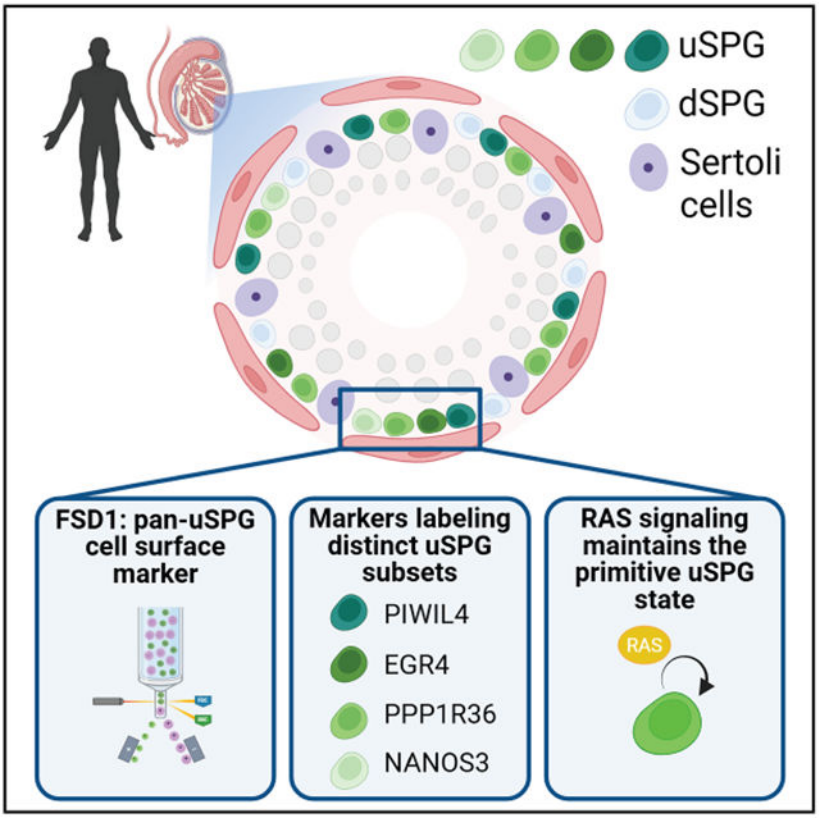

In brief

Capponi et al. define protein markers that distinguish human undifferentiated spermatogonial subsets and provide functional evidence that RAS signaling maintains their primitive state. This work establishes a framework for understanding human undifferentiated spermatogonial identity and regulation.

INTRODUCTION

Spermatogonial stem cells (SSCs) are essential for spermatogenesis and are promising agents to cure male subfertility and infertility, which afflicts 8%–12% of couples globally.[1] SSCs are a subset of undifferentiated spermatogonia (uSPG), a population that includes not only SSCs but also transit-amplifying progenitors. Traditionally, human uSPG have been classified into two distinct subsets—A_{dark} and A_{pale}—based on morphological criteria. A_{pale} cells are modestly proliferating uSPG, whereas A_{dark} cells are non- or rarely proliferative uSPG.[2,3] The function and relationship of these cell subsets are not known. A_{dark} and A_{pale}

cells may differ in their self-renewal capacity or may be the same cell type in different phases of the cell cycle.

Despite their clinical importance, human uSPG remain poorly understood at both the cellular and molecular levels. Toward a better understanding of uSPG, several uSPG markers have been identified and characterized to some extent.[4] For example, UCHL1 has been widely used as a pan-uSPG marker[5] and shows a conserved expression pattern in uSPG across species.[6] GFRA1 and UTF1 exhibit more selective expression within the uSPG compartment. GFRA1, the co-receptor for GDNF,[7] marks a subset of uSPG associated with proliferating cells in both nonhuman primates and humans,[8] while UTF1 is a chromatin-associated transcriptional repressor that labels quiescent uSPG that reflect a more primitive, reserve stem cell state.[4,8,9] Germ-cell transplantation analysis has identified several cell-surface proteins that label human SSCs, based on colony formation in mice testes, including $EpCAM^{low}$, $EpCAM^{low}$/HLA-ABC^{-}/$CD49e^{-}$, HLA-ABC^{-} /$CD9^{+}$, ITGA6, PLPPR3, and TSPAN33.[10-14] While these findings have provided tools for the study of human SSCs and transit-amplifying progenitors, the nature of the specific cell subsets labeled by these markers remains largely uncharacterized.

A powerful approach to characterize cell types and identify celltype- and stage-specific gene markers is single-cell RNA sequencing (scRNA-seq) analysis. In recent years, several groups, including ours, have used scRNA-seq analysis to investigate human spermatogenesis.[12,15-18] These single-cell-resolution studies revealed that there are multiple distinct uSPG cell clusters (i.e., cell subsets), each with different transcriptomes.[12,15,17,18] This suggested that uSPG are more heterogeneous than previously realized and led to the hypothesis that uSPG exist in distinct “states,” each with different properties. This hypothesis has remained largely untested. One possibility is that some scRNA-seq-defined cell clusters are a single population that is heterogeneous due to regulation by the cell cycle, epithelial cycle, or microenvironmental signals.[19] A non-mutually exclusive possibility is that one or more of these cell clusters have distinct functions, such as reserve vs. constitutive stem cell activity.[20-23]

As a foundational step to begin to address the heterogeneity of human uSPG, we leveraged recently defined human testis scRNA-seq datasets to screen for markers that label specific uSPG subsets. Many genes identified by these scRNA-seq studies were shown to be enriched in uSPG clusters,[12,15-18,24] raising the possibility that some of them could be valuable SSC and progenitor markers. While these findings were an important step forward toward defining uSPG markers, most of these candidate marker genes were not evaluated at the protein level. Even among those that were tested, characterization was largely limited to their broad spatial expression pattern within seminiferous tubules (e.g., center vs. periphery). Thus, their specificity or the nature of the cell populations recognized by these markers was unclear.

In this study, we employed a multi-pronged step-by-step strategy to identify uSPG marker proteins and characterize—in detail—the cell subsets labeled by these markers (Figure 1A). First, an *in silico* screen was performed to identify strong candidates from scRNA-seq datasets. Second, an antibody screen was conducted to identify antibodies and the

corresponding proteins that exhibited promising expression patterns, as determined by immunofluorescence analysis of human testis cross-sections. Third, to further assess their specificity, whole-mount immunostaining and multiplex labeling approaches were used for detailed characterization, including cross-comparison with previously defined markers. Fourth, to assess the relationship of the labeled cell subsets with classically defined uSPG cell populations (i.e., A_{dark} and A_{pale}), immunohistochemistry (IHC) analysis was performed. Fifth, cell sorting followed by transcriptomic profiling was conducted to molecularly characterize the entire uSPG population. Sixth, comparative transcriptomic analysis was conducted to define genes differentially expressed between different SPG subsets, leading to the identification of signaling pathways and transcriptional regulatory networks that are candidates with roles in determining uSPG fate. Finally, empirical experiments were performed that identified the RAS signaling pathway as playing a key role in human uSPG fate. Together, these findings provide a foundation for future studies that define the signaling networks governing human uSPG subset progression and for pre-clinical efforts to develop methods to purify and culture human SSCs toward the goal of curing male human infertility.

RESULTS

Identification of candidate markers specifically labeling human uSPG subsets

To identify uSPG marker proteins, we leveraged our adult human testis scRNA-seq study that identified 4 different uSPG cell clusters: SSC1-A, SSC1-B, SSC1-C, and SSC2.[18] While the developmental relationship of these 4 uSPG clusters is not known, pseudotime trajectory analysis suggested that the SSC1 clusters (particularly SSC1-B) represent the most primitive uSPG stages, while the SSC2 cluster represents an advanced uSPG stage poised to differentiate to the KIT^{high} stage of SPG[18] (Figure 1B). Genes exhibiting enriched expression were defined for each of these 4 uSPG cell clusters.[18] While these uSPG gene markers are useful for some applications, they have limitations, including that some markers label heterogeneous populations or are expressed in other testicular cell types, reducing their specificity. In addition, their encoding proteins are not expressed at the cell surface and thus cannot feasibly be used to purify the SPG subset(s) that they label. Thus, our initial goal in the present study was to screen the scRNA-seq-defined uSPG marker genes for those that encode proteins with specificity for uSPG, including *C19ORF81*, *C19ORF84*, *CAMK2B*, *CCK*, *CD82*, *CDH15*, *CELF4*, *CTSG*, *EGR4*, *ENO3*, *FGFR3*, *FSD1*, *GAL*, *ITLN1*, *NANOS2*, *NANOS3*, *PIWIL4*, *PPP1R36*, *SH2B2*, *SOCS1*, and *TMEM181* (Figure 1B). All of the genes we selected (1) exhibit specificity for distinct uSPG subsets, (2) have little or no expression in testicular somatic cells based on scRNA-seq analysis (Figure 1B),[18] and (3) include candidates encoding cell-surface proteins. While some candidate markers have been previously tested at the protein level in the human testis,[12,15-18,24] characterization was largely limited to broad spatial patterns within seminiferous tubules, necessitating further evaluation of their specificity for human uSPG.

Given that uSPG are specifically located at the periphery (directly adjacent to the basement membrane) of seminiferous tubules,[25] we first used immunofluorescence analysis of human testis sections to screen for uSPG genes that encode *bona fide* uSPG marker proteins. To

achieve this, we tested at least one commercial antibody per candidate marker; a total of 34 antibodies were tested. This screen identified antibodies against 5 proteins—EGR4, FSD1, NANOS3, PIWIL4, and PPP1R36—that label cells localized specifically at the periphery of seminiferous tubules (Figure 1C). Thus, we focused our subsequent detailed analysis on these 5 proteins, as described below. The antibodies against other proteins we tested (a total of 29 antibodies) either yielded little or no immunofluorescence signal or exhibited a much broader expression pattern than observed at the RNA level by scRNA-seq analysis (Figures 1C and S1), suggesting limited utility.

FSD1 is a cell-surface pan-uSPG marker enabling uSPG purification

Among the five candidate markers listed above, we first focused on FSD1, as it contains a fibronectin type III domain, which is commonly found in proteins that are secreted or localized to the cell surface,[26] raising the promising possibility that it could be used to purify uSPG. As support, fluorescence-activated cell sorting (FACS) analysis revealed that FSD1 labels approximately 9% of human testicular cells (Figure 2A).

To better characterize FSD1+ cells at the protein level, we performed whole-mount immunostaining analysis of human seminiferous tubules. Since scRNA-seq analysis showed that the *FSD1* gene is mainly expressed in the primitive uSPG subsets—SSC1-B and SSC1-C (Figure 1B)—we first assessed FSD1 protein expression by co-staining with GFRA1, UTF1, and PLPPR3, which are well-established uSPG markers.[3,8,13,18] Surprisingly, we found that FSD1 marks more cells than any of these uSPG markers (Figures 2B-2E, S2A, and S2B), indicating that it is a broad marker rather than a primitive uSPG marker. To test whether FSD1 expression is specific to SPG, we co-stained for MAGEA4, a pan-SPG marker,[27] and found that all FSD1+ cells are MAGEA4+ (Figures 2F and 2G). We next co-stained with UCHL1, a well-established pan-uSPG marker,[5] and found that there was a remarkable 97% overlap between FSD1+ and UCHL1+ cells (Figures 2H and 2I), suggesting that FSD1 is also a pan-uSPG marker. In support of its specificity, co-staining with KIT, a well-known differentiating SPG marker,[28] showed that FSD1+ cells exhibit only limited overlap with KIT+ cells (Figures 2J and 2K). This conclusion was also supported by our finding that FSD1 is expressed in a fraction (61%) of cells marked with the pan-SPG marker MAGEA4 (Figures 2F and 2G). Finally, we assessed the proliferation status of FSD1+ cells and found that 11% of these cells are MKI67+ (Figures S2C and S2D). Together, these findings revealed that FSD1 is a cell-surface marker that labels the majority of uSPG.

The developmental transcriptomic landscape of human uSPG

We next elected to leverage FSD1 as a means to purify uSPG and thereby uncover the molecular events occurring in human uSPG. We purified FSD1+ cells from the testes of four independent donors by FACS and performed bulk RNA-seq, which offers over 100-fold greater sequencing depth than scRNA-seq, enabling more sensitive detection of expressed genes. For comparison, bulk RNA-seq analysis was performed in parallel on unfractionated human testicular cells from the same donors.

Hierarchical clustering showed that the four FSD1+ uSPG samples clustered together, as did the four unfractionated samples, indicative of reproducible replicates (Figure 3A). Consistent with our above finding that FSD1 is an uSPG marker, FSD1+ cells exhibited highly enriched expression of known uSPG marker genes and de-enriched expression of advanced germ cell and somatic cell marker genes, as compared to unfractionated human testicular cells (Figure 3B). Compared to unfractionated cells, FSD1+ cells exhibit enriched expression of 3,766 genes ($q < 0.01$, fold change > 2; Table S1) that are significantly associated with the functions “cytokine,” “cell adhesion,” “cell activation,” “cell development,” and “MAPK cascade” (Figure 3C).

To uncover the molecular events potentially responsible for SPG development, we compared this uSPG (FSD1+) RNA-seq dataset with the differentiating SPG (KIT+) dataset we previously generated[13] (Figure 3D). Thousands of differentially expressed genes (DEGs) were identified ($q < 0.01$, fold change > 2; Figure 3D; Table S1). The DEGs enriched in FSD1+ cells are significantly associated with cell-surface receptor signaling, cell communication, and cell adhesion (Figure 3E), consistent with the possibility that extracellular signaling plays an essential role in maintaining the undifferentiated state of uSPG. By contrast, KIT+ cells are enriched with genes associated with metabolism processes, the cell cycle process, and the DNA damage response (Figure 3E), consistent with the fact that differentiating SPG are undergoing dynamic changes.[29,30]

Since transcription factors (TFs) are known to be essential for stem cell fate transitions,[31] we next evaluated which TF genes exhibit enriched expression. Among the 4,487 FSD1+ (uSPG)-enriched genes ($q < 0.01$, fold change >2), 269 encode TFs (Table S1). Among the 5,702 KIT+ (differentiating SPG)-enriched genes ($q < 0.01$, fold change > 2), 251 encode TFs (Table S1). To identify candidate TF regulatory networks, we used the gene set enrichment analysis (GSEA) program,[32] which identified FOXP2- and MAFG-mediated networks associated with FSD1+ uSPG, and PSMB5- and SETD7-mediated networks associated with KIT+ differentiating SPG (Figure 3F).

To decipher the molecular changes that occur as primitive uSPG transition into advanced uSPG, we made use of the RNA-seq dataset of human testicular cells expressing PLPPR3, which marks primitive uSPG and strongly enriches for SSCs by 38-fold, as assayed by the number of colonies formed upon transplantation into germ-cell-deficient mice.[13] Comparison of this dataset with that of FSD1+ cells (Figure 3G; Table S1) revealed that genes associated with cytokine, signaling transduction, and cell communication are enriched in PLPPR3+ cells (Figure 3H), raising the possibility that these functions are important for primitive uSPG. Genes associated with system and cell development, morphogenesis, and germ cell development are enriched in FSD1+ cells, implying that these functions may be involved in the transition of primitive uSPG to a more advanced state.

EGR4 and PPP1R36 distinguish quiescent and proliferating uSPG

We next turned our attention to the other uSPG markers we identified in our initial antibody screen. One of these markers was EGR4, which, at the RNA level, exhibits selective expression in SSC1, with predominant expression in SSC1-B, based on scRNA-seq analysis (Figure 1B). In contrast, IHC analysis revealed that the EGR4 protein is present in both

A_{pale} and A_{dark} uSPG (64% and 36%, respectively; Figure 4A), suggesting that it is not limited in its expression to primitive uSPG. To further characterize EGR4 expression, we performed whole-mount immunostaining analysis with known SPG markers. Our findings were as follows: first, EGR4 marks only a small subset of all SPG, based on its being co-expressed with only 17% MAGEA4+ cells (Figure 4B). Second, the vast majority of EGR4+ cells do not overlap with KIT+ cells (Figures S3A and S3B), consistent with scRNA-seq analysis showing that the EGR4 gene is primarily expressed in uSPG, not differentiating SPG (Figure 1B). Third, ~57% of EGR4+ cells co-express UTF1; these double-positive cells comprise 1/3 of the entire UTF1+ population (Figure 4C). Fourth, ~87% of EGR4+ SPG co-express GFRA1 (Figure 4D), which marks transitioning uSPG that are either poised for differentiation or are actively proliferating.[3,8] Fifth, MKI67 co-staining revealed that most EGR4+ uSPG are quiescent, with only 7% actively proliferating (Figure 4E), which is consistent with the co-expression of EGR4 and the “non-proliferating cell marker” UTF1 (Figure 4C). Of the few proliferating EGR4+ uSPG, all of them co-express GFRA1 (Figure S3C), indicating that EGR4 labels a small proliferative subset within the GFRA1+ population. Together, our results support a model in which EGR4 marks transition uSPG at the “cell proliferation gateway,” with (1) most being quiescent, (2) a subset primed for proliferation (those expressing GFRA1), and (3) an even smaller subset actively proliferating.

PPP1R36 is encoded by a gene that scRNA-seq analysis indicated is expressed in all 3 subclusters of the SSC1 cluster (Figure 1B), indicative of the *PPP1R36* gene being broadly expressed in uSPG. In contrast, our analysis of the PPP1R36 protein indicated that its expression is almost entirely restricted to A_{pale} SPG, with only 1% of PPP1R36+ cells having an A_{dark} morphology (Figure 4F). As further evidence of its restrictive expression, whole-mount immunostaining analysis showed that PPP1R36 expression is restricted to cells that express the pan-SPG marker MAGEA4 (Figure 4G). Of MAGEA4+ cells, only 37% express PPP1R36, providing further evidence of specificity. In apparent contrast with the rare expression of PPP1R36 RNA in differentiating SPG (Figure 1B), whole-mount immunostaining showed PPP1R36 protein in a subset of KIT+ differentiating SPG (Figure 4H). This raised the possibility that PPP1R36 labels not only uSPG but also some differentiating SPG. A resolution of this conundrum was provided by our finding that KIT expression is lower in PPP1R36+ KIT+ cells compared to PPP1R36− KIT+ cells (Figure S3D). This finding is consistent with the possibility that PPP1R36 marks the uSPG subset just beginning to express KIT as they transition toward becoming differentiating SPG.

Whole-mount immunostaining analysis also showed that PPP1R36 marks 33% of UTF1+ and 40% of GFRA1+ uSPG (Figures 4I and 4J). Notably, all PPP1R36+ UTF1+ cells also express GFRA1, suggesting that one subset of cells marked by PPP1R36 is non-proliferative uSPG primed to proliferate. Given that PPP1R36 also marks GFRA1+ cells that lack UTF1 expression, this raised the possibility that PPP1R36 also labels a subset of proliferative uSPG. Indeed, co-staining with MKI67 revealed that ~35% of PPP1R36+ cells were MKI67+ (Figure 4K), confirming that PPP1R36 labels proliferating SPG. Together, these results support a model in which PPP1R36 labels at least three classes of SPG, some of which may be overlapping subsets: (1) quiescent uSPG primed to proliferate, (2) a population of proliferating uSPG, and (3) differentiation-primed SPG.

To compare the expression of PPP1R36 with EGR4, we performed co-staining analysis with antibodies against both. Since both EGR4 and PPP1R36 are cytoplasmic and the antibodies against them are raised in rabbits, we employed a multiplexed protein labeling approach that conjugates antibodies with distinct fluorophores, enabling simultaneous analysis of both.[33] Using this approach, we observed a 34% overlap between these two markers (Figures S3E and S3F). Together, these findings allow us to outline the expression pattern of all tested SPG markers (Figure 4L).

PIWIL4 and NANOS3 label two distinct uSPG populations

scRNA-seq analysis performed by several groups has identified the *PIWIL4* gene as primarily being expressed in primitive uSPG.[12,15,17,18,24] Based on this, the corresponding protein has been used as a marker for primitive uSPG and SSCs in recent studies.[8,18,24] Here, we performed a detailed characterization of this marker. Whole-mount immunostaining showed that PIWIL4+ cells comprise 15% of all SPG (MAGEA4+ cells) (Figures 5A and 5B), and there is no overlap between PIWIL4+ and KIT+ cells (Figure S4A), confirming that PIWIL4 labels a subset of uSPG. Consistent with past studies showing that PIWIL4+ SPG are non-proliferative,[8,18,24] we found that all PIWIL4+ cells are MKI67− (Figure S4B). This observation is consistent with the finding that all PIWIL4+ cells express UTF1 (Figures 5C and 5D), a marker associated with uSPG quiescence.[8] While quiescent, 30% of PIWIL4+ cells express GFRA1 (Figures 5E and 5F), raising the possibility that a small subset of PIWIL4+ cells are primed for proliferation. Together, these findings support PIWIL4 as a quiescent primitive uSPG marker. Interestingly, IHC analysis revealed that the majority of PIWIL4+ cells (94%) are A_{pale} uSPG (Figures 5G and 5H), challenging the long-standing assumption that A_{dark} SPG represent the most primitive uSPG.

NANOS3 is the only "SSC2" marker for which we performed detailed protein-level characterization, and its RNA is primarily expressed in the SSC2 rather than the SSC1 cluster (Figure 1B). We found that the NANOS3 protein is expressed in a relatively small subset of SPG (only 15% of MAGEA4+ cells) (Figures 5I and 5J). A large proportion of NANOS3+ cells (46%) are actively proliferating (based on MKI67 co-staining; Figures 5K and 5L). Consistent with this, all NANOS3+ cells are A_{pale} SPG (Figure S4C), largely overlap with GFRA1+ uSPG (63%) (Figures 5K and 5L), and do not overlap with UTF1+ uSPG (Figure 5M).

To our knowledge, all currently established uSPG markers exhibit some overlapping expression. Given that the NANOS3 and PIWIL4 genes exhibit little or no overlapping expression at the RNA level (Figure 5N), they are candidates to encode nonoverlapping protein markers. Consistent with this possibility, the NANOS3 and PIWIL4 proteins have reciprocal expression patterns with respect to UTF1: all PIWIL4+ uSPG express UTF1 (Figures 5C and 5D), whereas no NANOS3+ uSPG express UTF1 (Figure 5M). Another difference between NANOS3 and PIWIL4 is that NANOS3 labels a small subset (12%) of KIT+ differentiating SPG that retain proliferative capacity (Figures 5O and 5P). Given that PPP1R36 also labels a small subset of KIT+ SPG, we performed co-staining and found that all NANOS3+ SPG co-express PPP1R36 (Figure S4D). Together, these findings provide a

compelling case that PIWIL4 and NANOS3 mark distinct subsets of uSPG, with PIWIL4 labeling primitive quiescent uSPG and NANOS3 labeling more advanced uSPG that are undergoing proliferation and/or committed to differentiation.

Figure 5Q provides a model that summarizes the expression pattern of the 5 protein markers we examined in detail in this study.

Evidence that the RAS signaling pathway promotes the uSPG primitive state

The identification of two distinct (non-overlapping) uSPG subpopulations provided an opportunity to identify genes and signaling pathways involved in uSPG fate transitions. In an initial attempt to achieve this, we performed bulk RNA-seq analysis on purified PIWIL4+ and NANOS3+ cells. Because neither of these markers is expressed on the cell surface, we enriched the corresponding uSPG populations through intracellular flow cytometry sorting, which requires cell fixation and permeabilization. Unfortunately, >90% of sequencing reads aligned to ribosome RNA, even when varying the number of PCR cycles (i.e., the library amplification step), probably as a result of the poor quality of RNA from the fixed cells. Given that this high ribosome RNA content could severely limit transcriptome coverage and compromise differential gene expression analysis, we decided not to rely on bulk RNA-seq analysis of enriched fixed cells to define DEGs.

As an alternative, we utilized our previously published scRNA-seq dataset[18] for this purpose. By comparing PIWIL4+ vs. NANOS3+ cells, we identified 1,072 and 554 genes exhibiting enriched expression in PIWIL4+ cells and NANOS3+ cells, respectively (Figure 6A; Table S1). PIWIL4-enriched genes are associated with “estrogen signaling,” “RAS signaling,” “focal adhesion,” “ErbB signaling,” “MAPK signaling,” and “VEGF signaling” pathways, while NANOS3-enriched genes are associated with “metabolic,” “nucleotide,” “oxidative phosphorylation,” “pentose phosphate,” “apoptosis,” and “cell cycle” pathways (Figure 6B).

We regarded the enrichment of the RAS pathway as particularly intriguing, as it is a key regulator of cell proliferation, survival, and differentiation,[34] making it a promising candidate pathway for stem cell maintenance and fate decisions. In addition, RAS signaling has been reported to trigger downstream pathways such as RAF-MEK-ERK and PI3K-AKT, both of which are important for maintaining SSCs in mice.[7,35,36] To empirically test whether the RAS pathway is essential for maintaining human PIWIL4+ uSPG fate, human uSPG were enriched using the pan-uSPG marker we identified in this study, FSD1 (Figure 2), and treated with RAS pathway inhibitors for 1 week (Figure 6C). For rigor, we tested two different well-established RAS inhibitors: lonafarnib[37] and salirasib.[38] Compared to vehicle-treated cells, both RAS inhibitors led to a significant reduction in the expression of the primitive uSPG marker, PIWIL4, and a significant upregulation of the expression of the advanced uSPG marker, NANOS3 (Figures 6D and 6E), consistent with driving the differentiation of the uSPG to a more advanced state. As an independent readout of RAS-signaling inhibition at the cell-population level, we analyzed testicular tissue fragment cultures by immunofluorescence staining (Figure 6C). We found that the number of PIWIL4+ cells and NANOS3+ cells per cross-section was markedly reduced and increased, respectively, upon incubation with the RAS inhibitors for 1 week (Figures

6F-6H). BrdU incorporation analysis showed no statistically significant changes in the proliferation status of either population, although NANOS3+ cells showed a trend toward increased BrdU labeling (Figures 6I and 6J). Together, these results demonstrate that inhibited RAS signaling drives uSPG to progress to a more advanced state, which implies that RAS signaling promotes the primitive uSPG state.

DISCUSSION

Human SSC therapy represents a promising strategy to treat male infertility. However, progress in this area has been hindered by the limited characterization of human SSCs, due in part to a scarcity of qualified specific markers. A further challenge is the growing evidence that SSCs may reside within multiple uSPG subpopulations. In this study, we sought to fill this gap by identifying and characterizing a panel of uSPG markers that resolve the heterogeneity within the human uSPG compartment, providing key insights into their molecular identity and potential function.

Through an integrated analysis of an scRNA-seq dataset and *in situ* protein validation, we identified PIWIL4, EGR4, PPP1R36, and NANOS3 as key markers that distinguish uSPG subpopulations. In addition, we identified FSD1 as a specific marker for the entire uSPG population. Notably, its localization to the cell surface makes FSD1 a valuable tool for the prospective purification of human uSPG. Indeed, using FSD1-based sorting, we purified human uSPG and performed transcriptomic profiling, which allowed us to uncover key molecular features underlying uSPG identity and function. For example, compared to KIT+ differentiating SPG, FSD1+ uSPG exhibit enrichment of pathways related to cell communication, adhesion, and receptor signaling, highlighting the potential importance of extracellular cues in maintaining the undifferentiated state of uSPG. In addition, in line with the well-established role of TFs in directing stem cell fate decisions,[31] we identified genes encoding distinct TF-regulatory networks that exhibit enriched expression in FSD1+ uSPG vs. KIT+ SPG. Elucidating the functional significance of these networks will require further empirical investigation to determine their roles in regulating human uSPG differentiation. Because of limited commercial antibody availability, we were unable to simultaneously isolate SPG populations defined by different markers. While cross-study comparisons of marker-labeled SPG populations may introduce bias, we minimized this by applying consistent protocols and analyzing multiple donors, thereby reducing variation. In our previous report, we identified FSD1 as a primitive uSPG marker,[18] based on RNA expression patterns (predicted by scRNA-seq analysis) and spatial protein distribution within seminiferous tubules (i.e., center vs. periphery). In the present study, we extend this observation by rigorously characterizing FSD1 through co-staining with several established SPG markers, demonstrating that FSD1 instead labels the entire uSPG population. This comprehensive characterization underscores the robustness of our approach and highlights the importance of rigorous marker validation for defining specificity in the field.

Our data indicate that PIWIL4 is a quiescent, primitive uSPG, a notion supported by previous studies.[8,18,24] Our comprehensive analysis revealed that its expression is confined to a rare subset of uSPG, with minimal overlap with GFRA1+ uSPG. Interestingly, only a small fraction of PIWIL4+ cells exhibit A_{dark} nuclear morphology, challenging the long-

standing assumption that A_{dark} SPG represent the most primitive uSPG. This observation is consistent with the notion proposed by Di Persio et al.[24] that A_{dark} cells comprise multiple uSPG states, not necessarily exclusively stem cells. This raises the possibility that the A_{dark} morphology is not a defining feature of human SSCs and that, instead, multiple uSPG states may exhibit A_{dark} morphology under specific conditions.

EGR4 marks a subset of uSPG that are predominantly quiescent, with a small fraction exhibiting proliferative activity. Our immunostaining analysis showed co-expression with GFRA1 and partial overlap with UTF1, suggesting that EGR4 labels a transitional uSPG state primed for proliferation and lineage commitment. Interestingly, EGR4 has been found to be upregulated in uSPG from cryptozoospermic patients compared to normal individuals,[24] which may have functional consequences given that EGR4 is known to govern a transcriptional regulatory network involved in cell proliferation and differentiation across multiple stem cell systems. In mice, there is evidence that EGR4 regulates multiple stages of spermatogenesis, as its loss leads to impaired meiosis progression, increased germ cell apoptosis, and progressive depletion of the SSC pool, ultimately leading to seminiferous tubule regression and germ cell loss.[39]

PPP1R36 marks a subset of proliferative uSPG with limited overlap with KIT+ differentiating SPG, suggesting that PPP1R36 labels early progenitor states rather than full, committed differentiating SPG. As support, KIT expression is lower in PPP1R36+ KIT+ cells than in PPP1R36− KIT+ cells (Figure S2D). Moreover, its partial overlapping expression with GFRA1 and its high co-expression with MKI67 support the idea that PPP1R36 is a proliferation marker and that proliferation coincides with the uSPG-to-differentiating-SPG transition.

We found that NANOS3 protein, encoded by a gene associated with primate uSPG and early progenitors,[18,40] is present in the majority (84%) of GFRA1+ proliferating uSPG. The absence of NANOS3 in a small fraction of GFRA1+ proliferating uSPG raises the possibility that these NANOS3− cells represent self-renewing SSCs, whereas NANOS3+ cells may correspond to expanding progenitors. Supporting this idea, in mice, *Nanos3* is expressed in most uSPG (A_{single} to $A_{aligned}$) and early differentiating A1 cells and has been proposed to function in transit-amplifying SPG rather than maintaining the stem cell pool.[41] Thus, NANOS3 may serve as a useful marker to distinguish proliferative fate within the GFRA1+ compartment; the latter is known to mark uSPG at the crossroads between self-renewal and differentiation.[8] Collectively, our observations allow us to propose a model for human uSPG identity. We consider that uSPG subsets may not represent fixed entities but rather exist in a dynamic equilibrium, consistent with one of the proposed models for uSPG replenishment.[42] For example, GFRA1+ cells may acquire NANOS3 expression to proliferate and expand the progenitor pool. Some of these progenitors may then proceed toward differentiation, whereas others could potentially re-acquire PIWIL4/UTF1 features, suggesting reversibility between quiescent and proliferative states.[8,24] We therefore depict this process as a circular rather than a strictly linear hierarchy to reflect these dynamic changes.

Our findings also provide mechanistic insights into the regulation of uSPG fate. We identified the RAS signaling pathway as a regulator of the transition between primitive and advanced uSPG. The RAS pathway appeared to only impact uSPG differentiation, not proliferation, as the overall proliferation rate of uSPG was not significantly altered. Future studies are needed to delineate the upstream activators and downstream targets of RAS signaling that mediate uSPG fate determination. Given its conserved roles in stem cell biology across many biological systems,[43-48] we speculate that the RAS signaling pathway serves as a central hub integrating several external cues to modulate stem cell fate decisions.

The mechanisms responsible for human SSC self-renewal vs. differentiation remain largely unclear. In rodents, GDNF and FGF2 are central to SSC maintenance, acting through RET, FGFR1, and downstream MAPK and PI3K pathways.[49,50] However, whether similar mechanisms apply to human SSCs remains largely untested. In our previous study,[13] we provided evidence that GDNF and BMP8B broadly support human SPG, while activin A selectively promotes human SPG differentiation. Of possible relevance toward maintaining and expanding human SSCs for clinical application, we found that inhibition of AKT signaling supported the maintenance of primitive human uSPG exhibiting a transcriptome characteristic of SSCs.[13] In the current study, we identify the RAS pathway as another candidate that promotes the maintenance of human primitive uSPG. It will be of interest to determine whether AKT inhibition and RAS signaling operate within the same regulatory network or act synergistically to support human uSPG maintenance.

Collectively, our study provides a refined molecular framework and a set of powerful markers for dissecting the heterogeneity and developmental dynamics of human uSPG. These findings not only advance our understanding of fundamental SSC biology but also offer valuable tools for translational research. Our study also has the potential to lay the groundwork for future translational efforts in SSC-based therapies.

Limitations of the study

While this study advances our understanding of human uSPG heterogeneity, the limitations outlined here define clear directions for future work. First, the limited availability of commercial antibodies restricted the simultaneous isolation of SPG populations defined by different markers, which may introduce bias when comparing across studies. We attempted to mitigate this by applying consistent protocols and analyzing samples from multiple donors, thereby strengthening reproducibility and robustness. Second, although FSD1 enabled purification of the entire uSPG population, key markers such as PIWIL4 and NANOS3 are intracellular and not yet suited for prospective isolation, limiting downstream functional assays. Optimization of intracellular sorting and RNA recovery, together with the development of corresponding cell-surface tools, will expand the ability to functionally interrogate discrete uSPG subsets. Third, transcriptomic profiling of FSD1+ cells revealed low-level somatic gene expression, most likely reflecting the minimal contamination inherent to bulk sorting. Future scRNA-seq analysis of purified FSD1+ cells would more precisely assess the specificity of FSD1 as a uSPG marker. Fourth, while our transcriptomic analyses highlighted candidate signaling pathways and TF networks, their mechanistic roles in uSPG state transitions remain to be fully elucidated. Our functional studies identified

RAS signaling as a regulator of the primitive uSPG state, but both upstream and downstream regulatory mechanisms warrant further investigation. Finally, the functional experiments were performed in short-term tissue fragment cultures, which do not fully recapitulate long-term human SSC maintenance or lineage potential. Future development of extended human SSC culture systems will be essential to validate the long-term fate and regenerative capacity of the identified uSPG subsets.

STAR★METHODS

EXPERIMENTAL MODEL AND STUDY PARTICIPANT DETAILS

Human testis samples preparation: Experiments involving human tissue were approved by the UCSD Human Research Protections Program (HRPP) under IRB-approved protocol #120471. Fresh testicular biopsies (from individuals aged 25–50 years) provided by Dr. Tung-Chin Hsieh (UCSD) were transported on ice to the research laboratory in Minimum Essential Medium Alpha (αMEM) supplemented with 10% FBS, within 1 h of collection. Upon arrival, samples were immediately cut into smaller pieces and, depending on the experimental need, either used for culture, fixed in 4% paraformaldehyde (PFA) or Bouin's solution (Sigma), or cryopreserved. For cryopreservation, tissue was frozen in a medium containing 10% DMSO, 40% αMEM, and 50% FBS, using a controlled-rate freezing container (Thermo Fisher Scientific) at −80°C. Samples were then transferred to liquid nitrogen for long-term storage. Additionally, testicular biopsies from 9 fertile men (aged 27, 28, 30, 34, 38, 38, 40, 40, and 46) were obtained through the University of Pittsburgh Health Sciences Tissue Bank and Center for Organ Recovery (CORID No. 686), provided by Dr. Kyle E. Orwig. All samples were deidentified.

METHOD DETAILS

Immunofluorescence analysis: As described previously,[13,18] human testis tissues were fixed overnight at 4°C on a nutator in 1× PBS containing 4% PFA (Sigma). Fixed samples were washed three times with cold PBS and embedded in paraffin. Paraffin sections were deparaffinized twice in xylene, followed by rehydration through a graded ethanol series. Antigen retrieval was performed in 10 mM sodium citrate buffer (pH 6.0) using a steamer (IHC WORLD) for 45 min. Blocking was performed by incubating the sections for 1 h at room temperature in 5% serum derived from the host species of the secondary antibody. Sections were then incubated overnight at 4°C with primary antibodies (Table S2). After three PBS washes, sections were incubated for 1 h at room temperature with species-specific secondary antibodies conjugated to Alexa 488 or Cy3 fluorochromes (Invitrogen). Nuclei were counterstained with DAPI, and sections were mounted with Vectashield mounting medium (Vector Laboratories). Images were acquired using a Leica DMI4000 B fluorescence microscope (Leica). Negative controls for all immunostaining experiments were performed by omitting the primary antibody to verify the specificity of the staining and rule out background signal from secondary reagents.

Whole Mount immunofluorescence: As described previously,[8,18] human seminiferous tubules were gently disentangled from testicular biopsies and immediately fixed in 4% PFA at 4°C for 4 h. Fixed tubules were permeabilized with 0.5% Triton X-100, treated with 1

M glycine for 1 h, and then incubated overnight at 4°C in PBS containing 0.1% Triton X-100, 1% bovine serum albumin (BSA), and 5% normal donkey serum. The following day, tubules were washed three times for 30 min in wash buffer (1% BSA, 0.1% Triton X-100 in PBS) and incubated overnight at 4°C with the appropriate primary antibodies (Table S2). Negative controls were prepared as described above. On the third day, tubules were washed as described above and incubated overnight at 4°C with species-specific secondary antibodies conjugated to Alexa 488, Cy3, or Cy5 fluorochromes (Invitrogen). For multiplexed protein labeling, as shown in Figures S2E and S3D, the FlexAble CoraLite Plus 555 kit (Proteintech, CatLog # KFA002) was used to label 0.5 μg of anti-PPP1R36 antibody, following the manufacturer's instructions. Both primary and secondary antibodies were diluted in PBS containing 1% BSA and 0.1% Triton X-100. Following secondary antibody incubation, tubules were washed, counterstained with DAPI, and mounted on slides using Vectashield mounting medium (Vector Laboratories). Imaging was performed using an Andor Dragonfly 200 Spinning Disk Confocal Microscope.

Immunohistochemical (IHC) analysis: As described previously,[8,18] IHC was performed on 5 μm-thick, Bouin's-fixed, paraffin-embedded human testis sections mounted on poly-L-lysine coated slides. Sections were deparaffinized twice in xylene and rehydrated through a graded ethanol series. Antigen retrieval was performed in 10 mM sodium citrate buffer (pH 6.0) using a steamer (IHC WORLD) for 45 min. Endogenous peroxidase activity was quenched by incubating the sections in 0.3% hydrogen peroxide in methanol for 15 min. Slides were then blocked in 3% serum (from the species in which the secondary antibody was raised) for 30 min at room temperature.

Sections were incubated overnight at 4°C with primary antibodies (Table S2), followed by incubation with the corresponding secondary antibody for 1 h at room temperature. Peroxidase activity was visualized using the Vectastain ABC kit and DAB (3,3′-diaminobenzidine tetrahydrochloride) substrate (Vector Laboratories). Nuclei were counterstained with Mayer's Hematoxylin (Sigma). After dehydration, coverslips were mounted with Eukitt mounting medium (Sigma), and images were acquired using an Olympus microscope. Negative controls were prepared as described above.

A_{dark} and A_{pale} SPG were identified based on nuclear morphology, as previously described.[57] Briefly, A_{dark} SPG exhibit a spherical or slightly ovoid nucleus with uniformly dark-stained chromatin and a characteristic unstained central rarefaction zone. In contrast, A_{pale} SPG display an ovoid nucleus with lightly stained chromatin and one to three deeply stained nucleoli adjacent to the nuclear envelope.

Fluorescence-activated cell sorting (FACS): Single testicular cells were isolated using a two-step enzymatic digestion protocol, as described previously.[13,18] Briefly, testicular tissue was mechanically minced and digested with 1 mg/mL collagenase type IV (Worthington Biochemical) in Hanks' Balanced Salt Solution (HBSS; Gibco) at 37°C. Following sedimentation and washing with HBSS, the tubules were subjected to a second digestion in 0.25% Trypsin-EDTA supplemented with Deoxyribonuclease I (Worthington Biochemical). The cell suspension was triturated vigorously ten times, incubated at 37°C for 5 min, and the trituration/incubation cycle was repeated once. Digestion was stopped by

adding an equal volume of αMEM containing 10% FBS. The cell suspension was filtered through 40 μm strainer (Thermo Fisher Scientific), and cells were pelleted by centrifugation at 300*g* for 5 min. Single cells were then resuspended in staining buffer (PBS + 3% FBS), incubated with the FSD1 primary antibody on ice for 20 min, washed, and incubated with a species-specific fluorophore-conjugated secondary antibody for 20 min on ice. After a final wash, cells were resuspended in staining buffer and sorted by FACS, as described previously.[13,18,58] Small debris and doublets were excluded based on forward and side scatter parameters. Unstained cells and cells stained with secondary antibody alone were used as negative controls to define background fluorescence and set gates for FSD1-positive populations.

Bulk RNA sequencing (RNAseq): RNAseq was performed as described previously.[13,58-62] Total RNA was extracted using the RNeasy Plus Micro Kit (Qiagen), following the manufacturer's protocol. 10 ng of total RNA was used to make the library using the SMART-Seq Total RNA Pico Input (Takara Bio), as per manufacturer's instructions. Libraries were sequenced (paired-end reads) with an Illumina NovaSeq X Plus platform for 100 cycles at the UCSD institute for Genomic Medicine (IGM) core.

Reads were filtered for quality and aligned with STAR (2.5.2b) against Homo sapiens, release-106, Ensembl genome (GRCh38). The exon counts were aggregated for each gene to build a read count table using SubRead function featureCounts. DEGs were defined using DESeq2 using the following threshold: $q < 0.01$, fold change > 2. The R package program, pheatmap, was used for clustering and generating heatmap plots. The Metascape platform was used for gene functional annotation using the following parameters: $p < 0.01$, minimum count of 3, and enrichment factor > 1.5.

Human FSD1+ cells culture: FSD1+ cells were enriched using magnetic-activated cell sorting (MACS), as described previously.[13] Briefly, human single testicular cells were resuspended in MACS buffer (PBS containing 0.5% BSA and 2 mM EDTA) and incubated with an anti-FSD1 antibody for 20 min on ice. After washing, cells were incubated with anti-rabbit IgG-conjugated microbeads (Miltenyi Biotec) for 20 min on ice. Cells were resuspended in 500 μL MACS buffer and loaded onto an MS column (Miltenyi Biotec). Following three washes with MACS buffer, FSD1+ cells were eluted and resuspended in culture medium. Approximately 1×10^5 sorted cells were plated per well in a 24-well plate pre-coated with laminin (20 μg/mL). For passaging, cells were incubated with StemPro Accutase (Gibco) for 5 min. FSD1+ cells were cultured under feeder-free conditions in a basal medium (IMDM/SFM) supplemented with 25 μg/mL insulin (Sigma), 100 μg/mL apo-Transferrin (Sigma), 200 μg/mL sodium pyruvate (Gibco), 60 μM putrescine (Sigma), 30 nM sodium selenite (Sigma), 6 mg/mL D-(+)-glucose (Sigma), 1 μL/mL DL-lactic acid (Sigma), 5 mg/mL bovine albumin (Sigma), 2 mM GlutaMAX supplement (Gibco), 50 μM 2-mercaptoethanol (Gibco), 1 × MEM vitamin solution (Gibco), 1 × non-essential amino acids (Gibco), 100 μM ascorbic acid (Sigma), 10 μg/mL day-Biotin (Sigma), 30 ng/mL β-Estradiol (Sigma), 60 ng/mL progesterone (Sigma), 1 mg/mL fetuin (Sigma), 10 μL/mL CD Lipid concentrate (Gibco), 2 μL/mL cholesterol solution (Sigma), and 50 μL/mL knockout serum replacement (Gibco). To support stem cell self-renewal, the medium

was supplemented with 10 ng/mL bFGF and 15 ng/mL recombinant human GDNF. For RAS pathway inhibition experiments, cells were cultured in this basal medium additionally supplemented with 5 μM Lonafarnib or 25 μM Salirasib (Selleck Chemicals).

RNA isolation and RT-qPCR analysis: Total RNA was extracted using the Direct-zol RNA MiniPrep Plus kit (Zymo Research), following the manufacturer's instructions. Complementary DNA (cDNA) was synthesized using the iScript reverse transcription kit (Bio-Rad). Quantitative real-time PCR was then performed using iQ SYBR Green Supermix (Vazyme) on an iCycler real-time PCR system, in accordance with the manufacturer's guidelines. The amplification of target genes was monitored through SYBR Green fluorescence, and threshold cycle (Ct) values were calculated. Expression levels were normalized to the housekeeping gene RPL19 (L19). Primers used in this study are detailed in Table S3.

Human testicular culture and BrdU incorporation: Fresh human testicular tissue was cut into 1 mm^3 pieces and placed into wells of a 12-well transwell plate (12 mm / 0.4 μm polyester membrane; Corning), and cultured at 34°C in 5% CO_2 with an air-liquid interface, as described previously.[63-65] The culture medium, which was replaced every 48 h, was the same as that used for human uSPG culture (as described above). For BrdU incorporation, tissue fragments were incubated for 2 h and 30 min with 25 μM 5-Bromo-2′-deoxyuridine (BrdU; Sigma). After incubation, the fragments were gently washed with PBS and fixed in 4% PFA at 4°C overnight before proceeding with immunofluorescence analysis, as described above.

Imaging and quantification: To quantify the relative proportions of SPG subtypes and their proliferation, intact seminiferous tubules from at least three different testicular samples were co-stained with relevant antibodies, as described previously.[8] Given the complex architecture of human seminiferous tubules, z-stacks were acquired to capture the entire SPG layer using an Andor Dragonfly 200 Spinning Disk Confocal Microscope with a 40x oil immersion objective. For each analysis, 15 fields (250.0 × 250.0 μm) were randomly selected from at least five different seminiferous tubules per sample. Confocal focus was achieved on the basal layer by examining nuclear staining. For each field, confocal z-stacks were captured with 1 μm increments between z slices. All representative immunofluorescence images shown in this study were processed as maximum intensity projections. SPG counts from human seminiferous tubules were normalized per field (250.0 × 250.0 μm). For immunofluorescence analysis of human testis sections, quantification was instead normalized per cross-section. The mean fluorescence intensity (MFI) of individual cells was measured using ImageJ Fiji. To determine the MFI, three non-fluorescent regions of interest (ROIs) were selected from the same image to calculate the background MFI. This background value was then subtracted from the MFI of ROIs manually drawn around single immunoreactive cells. Quantification was performed on stored images using ImageJ (Fiji) software. Details of all quantifications, including raw data, are provided in Table S4.

QUANTIFICATION AND STATISTICAL ANALYSIS

All quantitative data are presented as described in the figure legends. Normality and equal variance tests were performed for all variables. To assess the significance of differences between two independent groups, an unpaired two-tailed *t* test with a two-stage step-up false discovery rate (FDR) correction, according to Benjamini, Krieger, and Yekutieli, was applied. For comparisons among three independent groups, one-way analysis of variance (ANOVA) followed by a *post hoc* Tukey test was used. A p-value of < 0.05 was considered statistically significant. Statistical analyses were performed using SigmaPlot 14.0 and GraphPad Prism 9, and graphs were generated with GraphPad Prism 9 and R (version 4.3.1).

Supplementary Material

Refer to Web version on PubMed Central for supplementary material.

ACKNOWLEDGMENTS

We are grateful to Dr. Miles Wilkinson for helpful comments on the manuscript. We also thank the UC San Diego IGM Genomics Center for generating data on an Illumina NovaSeq X Plus that was purchased with funding from a National Institutes of Health (NIH) SIG grant (#S10 OD026929). We are also grateful to the San Diego Supercomputer Center for providing data analysis resources through allocation (BIO240308) from the Advanced Cyberinfrastructure Coordination Ecosystem: Services & Support (ACCESS) program, which is supported by US National Science Foundation grants #2138259, #2138286, #2138307, #2137603, and #2138296. This study was supported by NIH grant R01 GM119128 (K.T.) and the Lalor Institute (C.C.).

REFERENCES

1. Agarwal A, Baskaran S, Parekh N, Cho C-L, Henkel R, Vij S, Arafa M, Panner Selvam MK, and Shah R (2021). Male infertility. Lancet 397, 319–333. 10.1016/S0140-6736(20)32667-2. [PubMed: 33308486]
2. Clermont Y. (1972). Kinetics of spermatogenesis in mammals: seminiferous epithelium cycle and spermatogonial renewal. Physiol. Rev 52, 198–236. 10.1152/physrev.1972.52.1.198. [PubMed: 4621362]
3. Di Persio S, Saracino R, Fera S, Muciaccia B, Esposito V, Boitani C, Berloco BP, Nudo F, Spadetta G, Stefanini M, et al. (2017). Spermatogonial kinetics in humans. Development 144, 3430–3439. 10.1242/dev.150284. [PubMed: 28827392]
4. von Kopylow K, Kirchhoff C, Jezek D, Schulze W, Feig C, Primig M, Steinkraus V, and Spiess A-N (2010). Screening for biomarkers of spermatogonia within the human testis: a whole genome approach. Hum. Reprod 25, 1104–1112. 10.1093/humrep/deq053. [PubMed: 20208059]
5. Tokunaga Y, Imai S, Torii R, and Maeda T (1999). Cytoplasmic Liberation of Protein Gene Product 9.5 during the Seasonal Regulation of Spermatogenesis in the Monkey (Macaca fuscata). Endocrinology 140, 1875–1883. 10.1210/endo.140.4.6615. [PubMed: 10098527]
6. Boitani C, Di Persio S, Esposito V, and Vicini E (2016). Spermatogonial cells: mouse, monkey and man comparison. Semin. Cell Dev. Biol 59, 79–88. 10.1016/j.semcdb.2016.03.002. [PubMed: 26957475]
7. Meng X, Lindahl M, Hyvönen ME, Parvinen M, de Rooij DG, Hess MW, Raatikainen-Ahokas A, Sainio K, Rauvala H, Lakso M, et al. (2000). Regulation of cell fate decision of undifferentiated spermatogonia by GDNF. Science 287, 1489–1493. 10.1126/science.287.5457.1489. [PubMed: 10688798]
8. Capponi C, Palazzoli M, Di Persio S, Fera S, Spadetta G, Franco G, Wistuba J, Schlatt S, Neuhaus N, de Rooij D, and Vicini E (2023). Interplay of spermatogonial subpopulations during initial stages of spermatogenesis in adult primates. Development 150, dev201430. 10.1242/dev.201430. [PubMed: 37222410]

9. von Kopylow K, Staege H, Spiess A-N, Schulze W, Will H, Primig M, and Kirchhoff C (2012). Differential marker protein expression specifies rarefaction zone-containing human Adark spermatogonia. Reproduction 143, 45–57. 10.1530/REP-11-0290. [PubMed: 22046055]
10. Dovey SL, Valli H, Hermann BP, Sukhwani M, Donohue J, Castro CA, Chu T, Sanfilippo JS, and Orwig KE (2013). Eliminating malignant contamination from therapeutic human spermatogonial stem cells. J. Clin. Investig 123, 1833–1843. 10.1172/JCI65822. [PubMed: 23549087]
11. Nickkholgh B, Mizrak SC, van Daalen SKM, Korver CM, Sadri-Ardekani H, Repping S, and van Pelt AMM (2014). Genetic and epigenetic stability of human spermatogonial stem cells during long-term culture. Fertil. Steril 102, 1700–1707.e1. 10.1016/j.fertnstert.2014.08.022. [PubMed: 25256932]
12. Shami AN, Zheng X, Munyoki SK, Ma Q, Manske GL, Green CD, Sukhwani M, Orwig KE, Li JZ, and Hammoud SS (2020). Single-Cell RNA Sequencing of Human, Macaque, and Mouse Testes Uncovers Conserved and Divergent Features of Mammalian Spermatogenesis. Dev. Cell 54, 529–547.e12. 10.1016/j.devcel.2020.05.010. [PubMed: 32504559]
13. Tan K, Song H-W, Thompson M, Munyoki S, Sukhwani M, Hsieh T-C, Orwig KE, and Wilkinson MF (2020). Transcriptome profiling reveals signaling conditions dictating human spermatogonia fate in vitro. Proc. Natl. Acad. Sci. USA 117, 17832–17841. 10.1073/pnas.2000362117. [PubMed: 32661178]
14. Zohni K, Zhang X, Tan SL, Chan P, and Nagano M (2012). CD9 Is Expressed on Human Male Germ Cells That Have a Long-Term Repopulation Potential after Transplantation into Mouse Testes1. Biol. Reprod 87, 1–8. 10.1095/biolreprod.112.098913.
15. Guo J, Grow EJ, Mlcochova H, Maher GJ, Lindskog C, Nie X, Guo Y, Takei Y, Yun J, Cai L, et al. (2018). The adult human testis transcriptional cell atlas. Cell Res. 28, 1141–1157. 10.1038/s41422-018-0099-2. [PubMed: 30315278]
16. Hermann BP, Cheng K, Singh A, Roa-De La Cruz L, Mutoji KN, Chen I-C, Gildersleeve H, Lehle JD, Mayo M, Westernströer B, et al. (2018). The Mammalian Spermatogenesis Single-Cell Transcriptome, from Spermatogonial Stem Cells to Spermatids. Cell Rep. 25, 1650–1667.e8. 10.1016/j.celrep.2018.10.026. [PubMed: 30404016]
17. Wang M, Liu X, Chang G, Chen Y, An G, Yan L, Gao S, Xu Y, Cui Y, Dong J, et al. (2018). Single-Cell RNA Sequencing Analysis Reveals Sequential Cell Fate Transition during Human Spermatogenesis. Cell Stem Cell 23, 599–614.e4. 10.1016/j.stem.2018.08.007. [PubMed: 30174296]
18. Sohni A, Tan K, Song H-W, Burow D, de Rooij DG, Laurent L, Hsieh T-C, Rabah R, Hammoud SS, Vicini E, and Wilkinson MF (2019). The Neonatal and Adult Human Testis Defined at the Single-Cell Level. Cell Rep. 26, 1501–1517.e4. 10.1016/j.celrep.2019.01.045. [PubMed: 30726734]
19. Tan K, Song H-W, and Wilkinson MF (2020). Single-cell RNAseq analysis of testicular germ and somatic cell development during the perinatal period. Development 147, dev183251. 10.1242/dev.183251. [PubMed: 31964773]
20. Karmakar S, Deng L, He XC, and Li L (2020). Intestinal epithelial regeneration: active versus reserve stem cells and plasticity mechanisms. Am. J. Physiol. Gastrointest. Liver Physiol 318, G796–G802. 10.1152/ajpgi.00126.2019. [PubMed: 32003604]
21. Tan K, Jones SH, Lake BB, Chousal JN, Shum EY, Zhang L, Chen S, Sohni A, Pandya S, Gallo RL, et al. (2020). The role of the NMD factor UPF3B in olfactory sensory neurons. eLife 9, e57525. 10.7554/eLife.57525. [PubMed: 32773035]
22. Morrison SJ, and Spradling AC (2008). Stem Cells and Niches: Mechanisms That Promote Stem Cell Maintenance throughout Life. Cell 132, 598–611. 10.1016/j.cell.2008.01.038. [PubMed: 18295578]
23. Tan K, and Wilkinson MF (2020). A single-cell view of spermatogonial stem cells. Curr. Opin. Cell Biol 67, 71–78. 10.1016/j.ceb.2020.07.005. [PubMed: 32950921]
24. Di Persio S, Tekath T, Siebert-Kuss LM, Cremers J-F, Wistuba J, Li X, Meyer Zu Hörste G, Drexler HCA, Wyrwoll MJ, Tüttelmann F, et al. (2021). Single-cell RNA-seq unravels alterations of the human spermatogonial stem cell compartment in patients with impaired spermatogenesis. Cell Rep. Med 2, 100395. 10.1016/j.xcrm.2021.100395. [PubMed: 34622232]

25. De Rooij DG, and Russell LD (2000). All You Wanted to Know About Spermatogonia but Were Afraid to Ask. J. Androl 21, 776–798. 10.1002/j.1939-4640.2000.tb03408.x. [PubMed: 11105904]
26. Dalton CJ, and Lemmon CA (2021). Fibronectin: Molecular Structure, Fibrillar Structure and Mechanochemical Signaling. Cells 10, 2443. 10.3390/cells10092443. [PubMed: 34572092]
27. Aubry F, Satie A-P, Rioux-Leclercq N, Rajpert-De Meyts E, Spagnoli GC, Chomez P, De Backer O, Jégou B, and Samson M, (2001). MAGE-A4, a germ cell specific marker, is expressed differentially in testicular tumors. Cancer 92, 2778–2785. 10.1002/1097-0142(20011201)92:11<2778::AID-CNCR10125>3.0.CO;2-S. [PubMed: 11753951]
28. Schrans-Stassen BH, van de Kant HJ, de Rooij DG, and van Pelt AM (1999). Differential Expression of c-kit in Mouse Undifferentiated and Differentiating Type A Spermatogonia. Endocrinology 140, 5894–5900. 10.1210/endo.140.12.7172. [PubMed: 10579355]
29. Zhang Z, Miao J, Wang H, Ali I, Nguyen D, Chen W, and Wang Y (2024). Accelerated mitochondrial dynamics promote spermatogonial differentiation. Stem Cell Rep. 19, 1548–1563. 10.1016/j.stemcr.2024.09.006.
30. Zheng Y, Zhang L, Jin L, Zhang P, Li F, Guo M, Gao Q, Zeng Y, Li M, and Zeng W (2022). Unraveling three-dimensional chromatin structural dynamics during spermatogonial differentiation. J. Biol. Chem 298, 101559. 10.1016/j.jbc.2021.101559. [PubMed: 34979097]
31. Joung J, Ma S, Tay T, Geiger-Schuller KR, Kirchgatterer PC, Verdine VK, Guo B, Arias-Garcia MA, Allen WE, Singh A, et al. (2023). A transcription factor atlas of directed differentiation. Cell 186, 209–229.e26. 10.1016/j.cell.2022.11.026. [PubMed: 36608654]
32. Subramanian A, Tamayo P, Mootha VK, Mukherjee S, Ebert BL, Gillette MA, Paulovich A, Pomeroy SL, Golub TR, Lander ES, and Mesirov JP (2005). Gene set enrichment analysis: a knowledgebased approach for interpreting genome-wide expression profiles. Proc. Natl. Acad. Sci. USA 102, 15545–15550. 10.1073/pnas.0506580102. [PubMed: 16199517]
33. Tan WCC, Nerurkar SN, Cai HY, Ng HHM, Wu D, Wee YTF, Lim JCT, Yeong J, and Lim TKH (2020). Overview of multiplex immunohistochemistry/immunofluorescence techniques in the era of cancer immunotherapy. Cancer Commun. 40, 135–153. 10.1002/cac2.12023.
34. Molina JR, and Adjei AA (2006). The Ras/Raf/MAPK Pathway. J. Thorac. Oncol 1, 7–9. 10.1016/S1556-0864(15)31506-9. [PubMed: 17409820]
35. Kubota H, Avarbock MR, and Brinster RL (2004). Growth factors essential for self-renewal and expansion of mouse spermatogonial stem cells. Proc. Natl. Acad. Sci. USA 101, 16489–16494. 10.1073/pnas.0407063101. [PubMed: 15520394]
36. Oatley JM, Avarbock MR, and Brinster RL (2007). Glial Cell Line-derived Neurotrophic Factor Regulation of Genes Essential for Selfrenewal of Mouse Spermatogonial Stem Cells Is Dependent on Src Family Kinase Signaling. J. Biol. Chem 282, 25842–25851. 10.1074/jbc.M703474200. [PubMed: 17597063]
37. Basso AD, Mirza A, Liu G, Long BJ, Bishop WR, and Kirschmeier P (2005). The Farnesyl Transferase Inhibitor (FTI) SCH66336 (lonafarnib) Inhibits Rheb Farnesylation and mTOR Signaling: Role in Fti Enhancement of Taxane and Tamoxifen Anti-Tumor Activity. J. Biol. Chem 280, 31101–31108. 10.1074/jbc.M503763200. [PubMed: 16006564]
38. Gana-Weisz M, Haklai R, Marciano D, Egozi Y, Ben-Baruch G, and Kloog Y (1997). The Ras AntagonistS-Farnesylthiosalicylic Acid Induces Inhibition of MAPK Activation. Biochem. Biophys. Res. Commun 239, 900–904. 10.1006/bbrc.1997.7582. [PubMed: 9367867]
39. Hogarth CA, Mitchell D, Small C, and Griswold M (2010). EGR4 displays both a cell- and intracellular-specific localization pattern in the developing murine testis. Dev. Dyn 239, 3106–3114. 10.1002/dvdy.22442. [PubMed: 20925118]
40. Lau X, Munusamy P, Ng MJ, and Sangrithi M (2020). Single-Cell RNA Sequencing of the Cynomolgus Macaque Testis Reveals Conserved Transcriptional Profiles during Mammalian Spermatogenesis. Dev. Cell 54, 548–566.e7. 10.1016/j.devcel.2020.07.018. [PubMed: 32795394]
41. Suzuki H, Sada A, Yoshida S, and Saga Y (2009). The heterogeneity of spermatogonia is revealed by their topology and expression of marker proteins including the germ cell-specific proteins Nanos2 and Nanos3. Dev. Biol 336, 222–231. 10.1016/j.ydbio.2009.10.002. [PubMed: 19818747]
42. de Rooij DG (2017). The nature and dynamics of spermatogonial stem cells. Development 144, 3022–3030. 10.1242/dev.146571. [PubMed: 28851723]

43. Jiang H, and Edgar BA (2009). EGFR signaling regulates the proliferation of Drosophila adult midgut progenitors. Development 136, 483–493. 10.1242/dev.026955. [PubMed: 19141677]
44. Yanagisawa M, Nakamura K, and Taga T (2005). Glycosphingolipid synthesis inhibitor represses cytokine-induced activation of the Ras-MAPK pathway in embryonic neural precursor cells. J. Biochem 138, 285–291. 10.1093/jb/mvi129. [PubMed: 16169879]
45. Gierut JJ, Lyons J, Shah MS, Genetti C, Breault DT, and Haigis KM (2015). Oncogenic K-Ras Promotes Proliferation in Quiescent Intestinal Stem Cells. Stem Cell Res. 15, 165–171. 10.1016/j.scr.2015.06.003. [PubMed: 26079371]
46. Bender RHF, Haigis KM, and Gutmann DH (2015). Activated K-Ras, but Not H-Ras or N-Ras, Regulates Brain Neural Stem Cell Proliferation in a Raf/Rb-Dependent Manner. Stem Cell. 33, 1998–2010. 10.1002/stem.1990.
47. He Z, Jiang J, Kokkinaki M, Golestaneh N, Hofmann M-C, and Dym M (2008). Gdnf upregulates c-Fos transcription via the Ras/Erk1/2 pathway to promote mouse spermatogonial stem cell proliferation. Stem Cell. 26, 266–278. 10.1634/stemcells.2007-0436.
48. Fatrai S, van Gosliga D, Han L, Daenen SMGJ, Vellenga E, and Schuringa JJ (2011). KRASG12V Enhances Proliferation and Initiates Myelomonocytic Differentiation in Human Stem/Progenitor Cells via Intrinsic and Extrinsic Pathways. J. Biol. Chem 286, 6061–6070. 10.1074/jbc.M110.201848. [PubMed: 21169357]
49. Song H-W, and Wilkinson MF (2014). Transcriptional control of spermatogonial maintenance and differentiation. Semin. Cell Dev. Biol 30, 14–26. 10.1016/j.semcdb.2014.02.005. [PubMed: 24560784]
50. Suzuki S, McCarrey JR, and Hermann BP (2021). An mTORC1-dependent switch orchestrates the transition between mouse spermatogonial stem cells and clones of progenitor spermatogonia. Cell Rep. 34, 108752. 10.1016/j.celrep.2021.108752. [PubMed: 33596419]
51. Dobin A, Davis CA, Schlesinger F, Drenkow J, Zaleski C, Jha S, Batut P, Chaisson M, and Gingeras TR (2013). STAR: ultrafast universal RNA-seq aligner. Bioinforma. Oxf. Engl 29, 15–21. 10.1093/bioinformatics/bts635.
52. Liao Y, Smyth GK, and Shi W (2014). featureCounts: an efficient general purpose program for assigning sequence reads to genomic features. Bioinforma. Oxf. Engl 30, 923–930. 10.1093/bioinformatics/btt656.
53. Love MI, Huber W, and Anders S (2014). Moderated estimation of fold change and dispersion for RNA-seq data with DESeq2. Genome Biol 15, 550. 10.1186/s13059-014-0550-8. [PubMed: 25516281]
54. Kolde R. (2025). pheatmap: Pretty Heatmaps. R package version 1.0.13.https://github.com/raivokolde/pheatmap.
55. Zhou Y, Zhou B, Pache L, Chang M, Khodabakhshi AH, Tanaseichuk O, Benner C, and Chanda SK (2019). Metascape provides a biologist-oriented resource for the analysis of systems-level datasets. Nat. Commun 10, 1523. 10.1038/s41467-019-09234-6. [PubMed: 30944313]
56. Schindelin J, Arganda-Carreras I, Frise E, Kaynig V, Longair M, Pietzsch T, Preibisch S, Rueden C, Saalfeld S, Schmid B, et al. (2012). Fiji: an open-source platform for biological-image analysis. Nat. Methods 9, 676–682. 10.1038/nmeth.2019. [PubMed: 22743772]
57. Clermont Y. (1966). Renewal of spermatogonia in man. Am. J. Anat 118, 509–524. 10.1002/aja.1001180211. [PubMed: 5917196]
58. Tan K, Sebat J, and Wilkinson MF (2025). Cell type- and factor-specific nonsense-mediated RNA decay. Nucleic Acids Res. 53, gkaf395. 10.1093/nar/gkaf395. [PubMed: 40366162]
59. Tan K, and Wilkinson MF (2022). Regulation of both transcription and RNA turnover contribute to germline specification. Nucleic Acids Res. 50, 7310–7325. 10.1093/nar/gkac542. [PubMed: 35776114]
60. Tan K, Song H-W, and Wilkinson MF (2021). RHOX10 drives mouse spermatogonial stem cell establishment through a transcription factor signaling cascade. Cell Rep. 36, 109423. 10.1016/j.cel-rep.2021.109423. [PubMed: 34289349]
61. Tan K, Kim ME, Song H-W, Skarbrevik D, Babajanian E, Bedrosian TA, Gage FH, and Wilkinson MF (2021). The Rhox gene cluster suppresses germline LINE1 transposition. Proc. Natl. Acad. Sci. USA 118, e2024785118. 10.1073/pnas.2024785118. [PubMed: 34083437]

62. Tan K, Higgins K, Liu Q, and Wilkinson MF (2025). An ancient enhancer rapidly evolving in the human lineage promotes neural development and cognitive flexibility. Sci. Adv 11, eadt0534. 10.1126/sciadv.adt0534. [PubMed: 40802760]

63. Curaba M, Poels J, van Langendonckt A, Donnez J, and Wyns C (2011). Can prepubertal human testicular tissue be cryopreserved by vitrification? Fertil. Steril 95, 2123.e9–12. 10.1016/j.fertnstert.2011.01.014.

64. de Michele F, Poels J, Giudice MG, De Smedt F, Ambroise J, Vermeulen M, Gruson D, and Wyns C (2018). In vitro formation of the blood–testis barrier during long-term organotypic culture of human prepubertal tissue: comparison with a large cohort of pre/peripubertal boys. Mol. Hum. Reprod 24, 271–282. 10.1093/molehr/gay012. [PubMed: 29538744]

65. Younis N, Caldeira-Brant AL, Chu T, Abdalla S, and Orwig KE (2023). Human immature testicular tissue organ culture: a step towards fertility preservation and restoration. Front. Endocrinol 14, 1242263. 10.3389/fendo.2023.1242263.

Highlights

- FSD1 enables purification of all undifferentiated spermatogonia (uSPG)
- EGR4 and PPP1R36 distinguish quiescent and proliferating uSPG
- PIWIL4 and NANOS3 mark two clearly separable uSPG populations
- RAS signaling is critical for maintaining the primitive uSPG identity

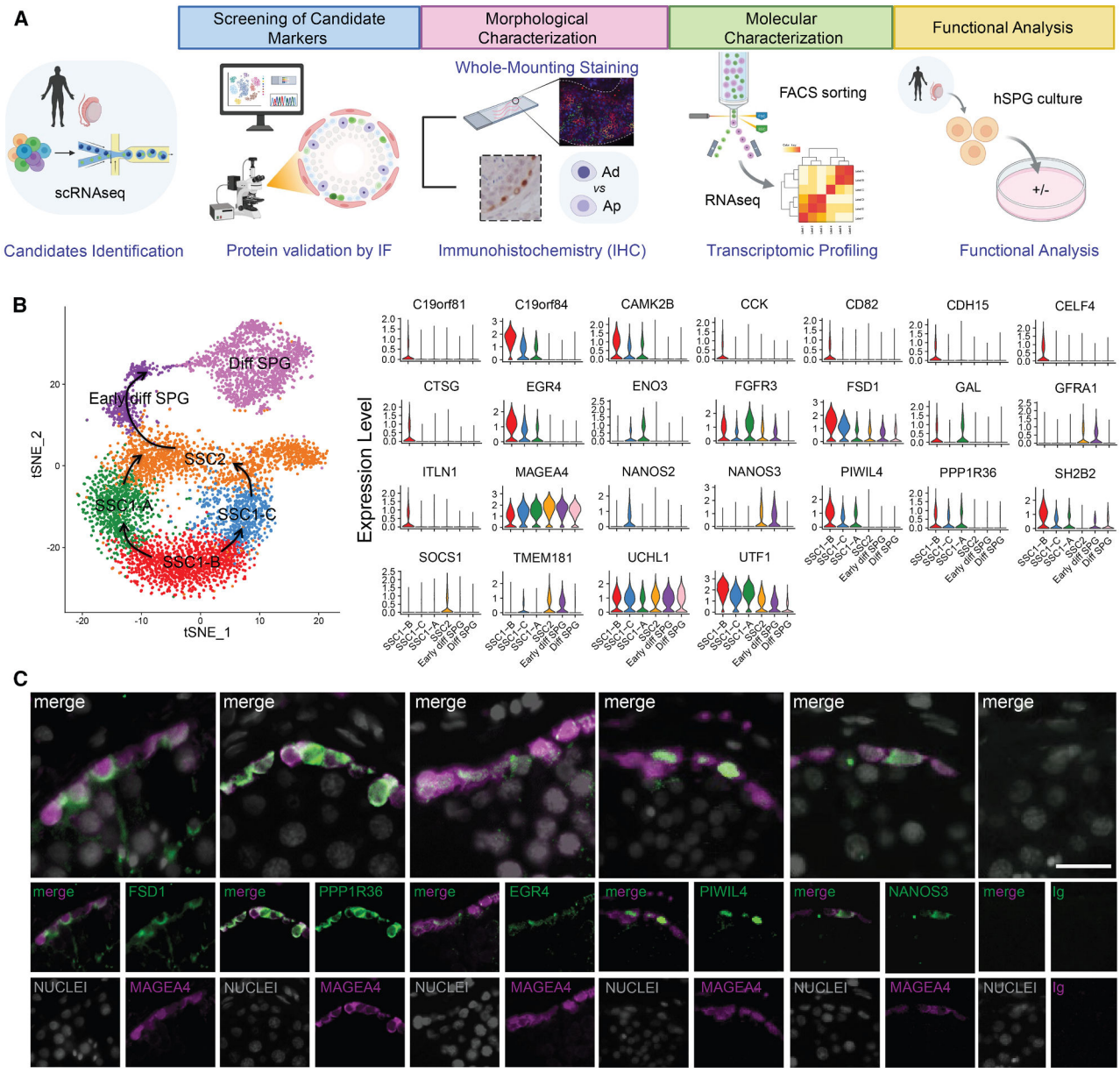

Figure 1. Identification of candidate markers specifically labeling human undifferentiated SPG subsets

(A) Experimental outline. A multi-pronged strategy was used to identify and characterize human uSPG markers and investigate their developmental regulation, as detailed in the text.

(B) Left, t-distributed stochastic neighbor embedding (tSNE) plot showing SPG subsets identified from scRNA-seq analysis.[18] Right, violin plots showing expression of candidate markers across the annotated SPG clusters.

(C) Representative images of immunofluorescence analysis of human testis sections stained with the indicated antisera against candidate markers (green). The pan-SPG marker MAGEA4 was co-stained (magenta), and cell nuclei were counterstained with DAPI (gray). The negative control (Ig) shows sections stained with the secondary antibody only. Scale bars: 20 μm.

See also Figure S1.

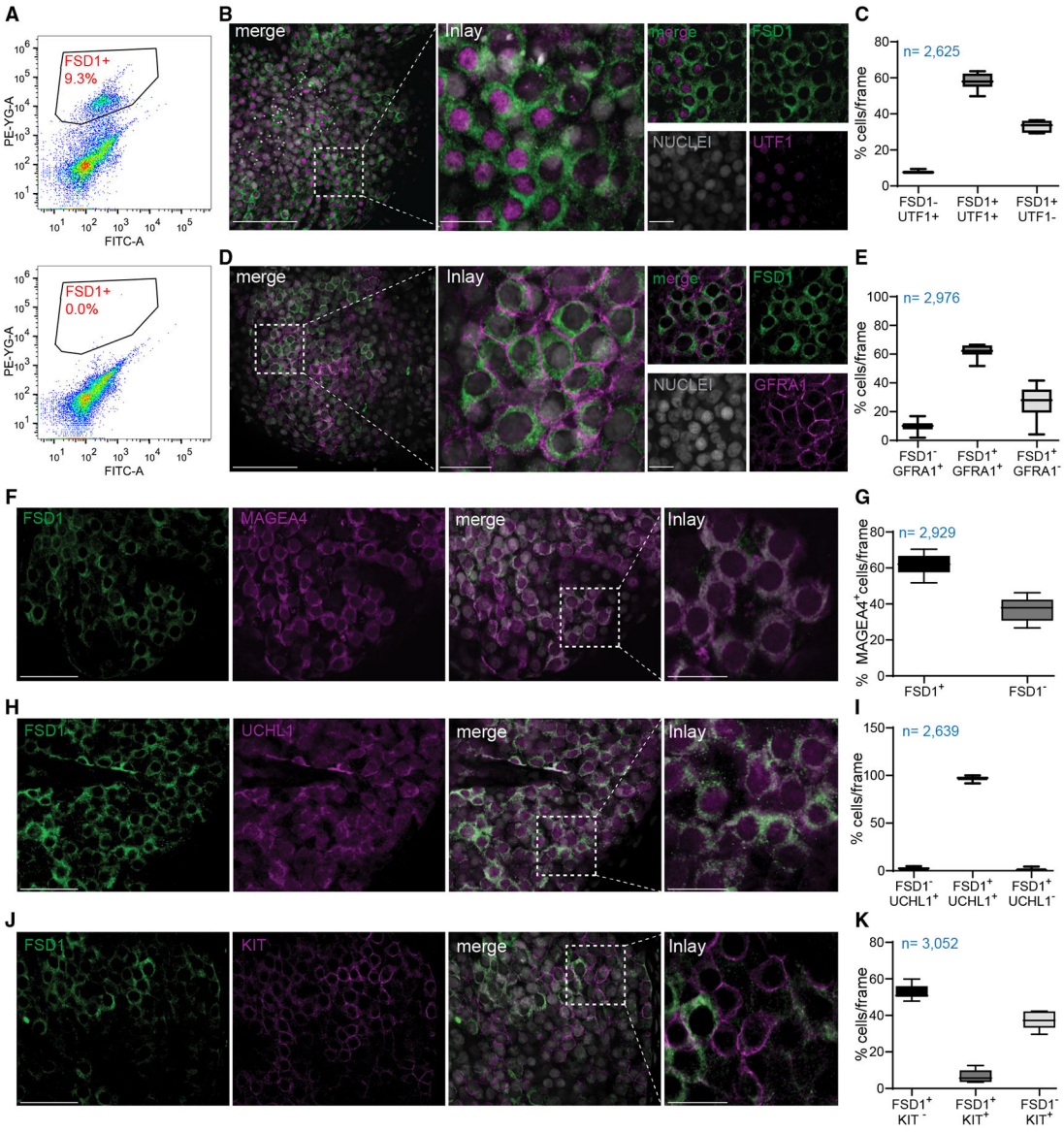

Figure 2. FSD1 is a cell-surface pan-uSPG marker enabling uSPG purification

(A) FACS plot of human adult testicular cells stained with antisera against FSD1, followed by labeled secondary antisera (top) or secondary antisera alone (bottom).

(B, D, F, H, and J) Representative images of whole-mount human testicular seminiferous tubules stained with antisera against FSD1 (green) and the indicated markers (magenta). Cell nuclei were counterstained with DAPI (gray). Testicular samples from 3 fertile individuals were analyzed. Scale bars: (B and D) 100 μm and 20 μm (insets), (F, H, and J) 50 μm and 20 μm (insets).

(C, E, G, I, and K) Quantification of positive cells that co-stain or not, as indicated. *n*, the total number of SPG counted. Boxplot elements: center line, median; box limits, upper and lower quartiles; whiskers, 1.5× interquartile range; points, outliers.

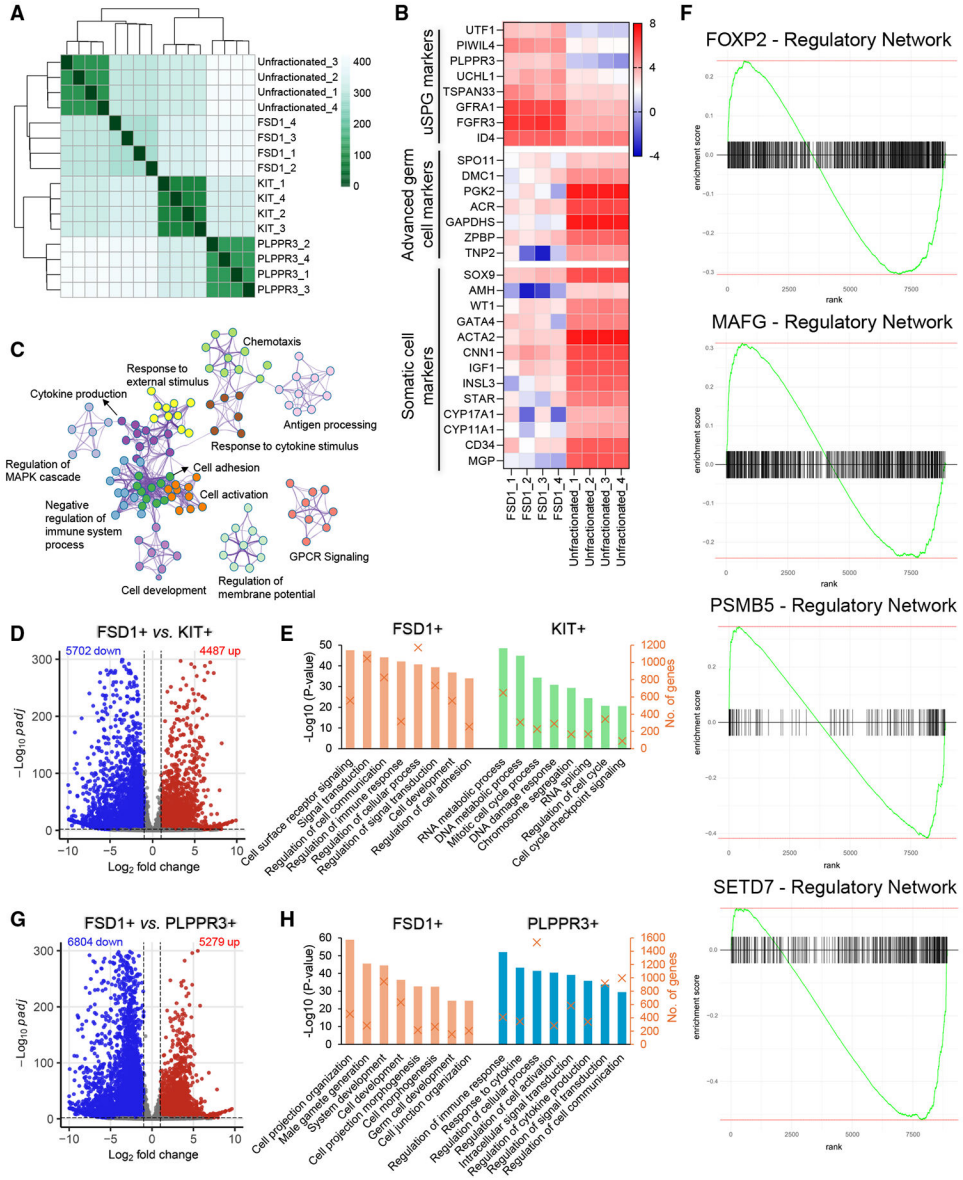

Figure 3. Identification of the developmental transcriptomic landscape of human uSPG

(A) Unsupervised hierarchical clustering of RNA-seq datasets from unfractionated human testicular cells and purified SPG subsets using the indicated markers. Four biological replicates were obtained from fertile individuals (aged 28, 30, 34, and 40 years).

(B) Heatmap of gene markers for uSPG, advanced germ cells, and somatic cells. All four biological replicates for each group are shown.

(C) Biological functions defined by the Metascape program ($p < 0.01$) associated with genes enriched in FSD1+ cells ($q < 0.01$, fold change > 2).

(D) Differentially expressed genes (DEGs; $q < 0.01$, fold change > 2) from FSD1+ vs. KIT+ cells.

(E) Biological functions associated with the DEGs defined in (D). Statistical significance (−log10 (p value)) is indicated by the bar. The number of DEGs for a given category is indicated by an “X.”.

(F) Top 2 transcription factor (TF) regulatory networks identified by GSEA program: FOXP2- and MAFG-mediated networks enriched in FSD1+ uSPG, and PSMB5- and SETD7-mediated networks enriched in KIT+ differentiating SPG.
(G) DEGs ($q < 0.01$, fold change > 2) from FSD1+ vs. PLPPR3+ cells.
(H) Biological functions associated with the DEGs defined in (G). Statistical significance (−log10 (*p* value)) is indicated by the bar. The number of DEGs for a given category is indicated by an "X."

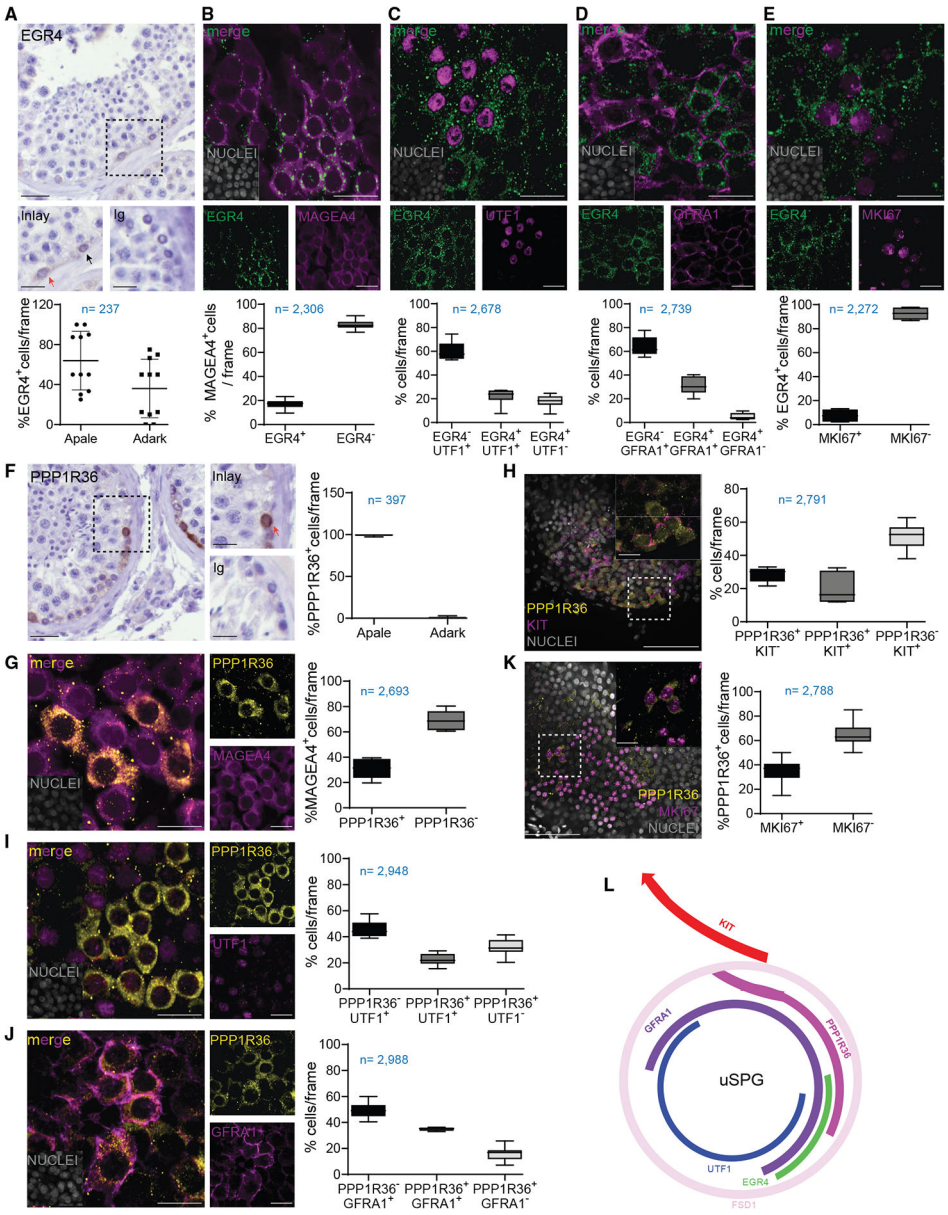

Figure 4. EGR4 and PPP1R36 distinguish quiescent and proliferating uSPG

(A) Top, immunohistochemistry (IHC) analysis of EGR4 on human testis sections. The negative control (Ig) shows sections stained with the secondary antibody only. Scale bars: 50 μm (low magnification) and 20 μm (high magnification). Black arrow, A_{dark} SPG; orange arrow, A_{pale} SPG. Bottom, quantification of A_{pale} and A_{dark} EGR4+ SPG. Testicular samples from 3 fertile individuals were analyzed.

(B–E) Top, representative images of whole-mount human seminiferous tubules stained with antisera against EGR4 (green) and the indicated markers (magenta). Nuclei were counterstained with DAPI (gray). Testicular samples from 3 fertile individuals were analyzed. Scale bars: 20 μm. Bottom, quantification of positive cells that co-stain or not, as indicated. *n*, the total number of SPG counted. Boxplot elements: center line, median; box limits, upper and lower quartiles; whiskers, 1.5× interquartile range; points, outliers.

(F) Left, IHC analysis of PPP1R36 on human testis sections. The negative control (Ig) shows sections stained with the secondary antibody only. Scale bars: 50 μm (low magnification) and 20 μm (high magnification). Orange arrow, A_{pale} SPG. Right, quantification of A_{pale} and A_{dark} PPP1R36+ SPG. Testicular samples from 3 fertile individuals were analyzed.
(G–K) Left, representative images of whole-mount human seminiferous tubules stained with antisera against PPP1R36 (yellow) and the indicated markers (magenta). Nuclei were counterstained with DAPI (gray). Testicular samples from 3 fertile individuals were analyzed. Scale bars: (G, I, and J) 20 μm, (H and K) 100 μm and 20 μm (insets). Right, quantification of positive cells that co-stain or not, as indicated. *n*, the total number of SPG counted. Boxplot elements: center line, median; box limits, upper and lower quartiles; whiskers, 1.5× interquartile range; points, outliers.
(L) Schematic model of the human SPG compartment highlighting distinct subsets marked by EGR4 and PPP1R36
See also Figure S2.

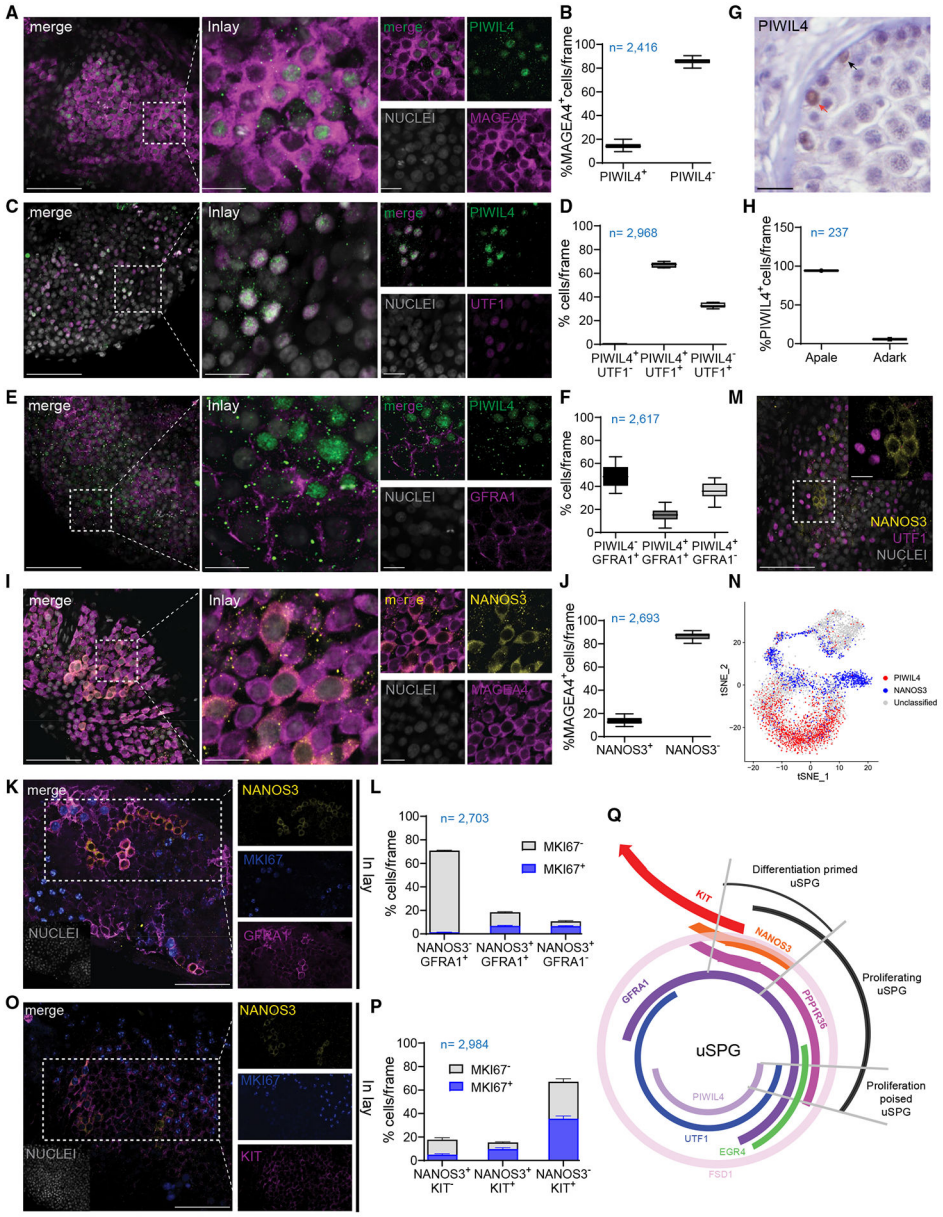

Figure 5. PIWIL4 and NANOS3 label two distinct uSPG populations

(A, C, and E) Representative images of whole-mount human seminiferous tubules stained with antisera against PIWIL4 (green) and the indicated markers (magenta). Nuclei were counterstained with DAPI (gray). Testicular samples from 3 fertile individuals were analyzed. Scale bars: 100 μm and 20 μm (insets).

(B, D, and F) Quantification of positive cells that co-stain or not, as indicated. *n*, the total number of SPG counted. Boxplot elements: center line, median; box limits, upper and lower quartiles; whiskers, 1.5× interquartile range; points, outliers.

(G) IHC analysis of PIWIL4 on human testis sections. Scale bars: 50 μm. Black arrow, A_{dark} SPG; orange arrow, A_{pale} SPG.

(H) Quantification of A_{pale} and A_{dark} PIWIL4+ SPG. Testicular samples from 3 fertile individuals were analyzed.

(I, K, M, and O) Representative images of whole-mount human seminiferous tubules stained with antisera against NANOS3 (yellow) and the indicated markers (magenta). Nuclei were counterstained with DAPI (gray). Testicular samples from 3 fertile individuals were analyzed. Scale bars: 100 μm and 20 μm (insets).

(J, L, and P) Quantification of positive cells that co-stain or not, as indicated. *n*, the total number of SPG counted. Boxplot elements: center line, median; box limits, upper and lower quartiles; whiskers, 1.5× interquartile range; points, outliers.

(N) tSNE plot showing PIWIL4 and NANOS3 expression across SPG clusters from scRNA-seq analysis.

(Q) Schematic model of the human SPG compartment based on the expression of EGR4, PPP1R36, PIWIL4, and NANOS3.

See also Figure S3.

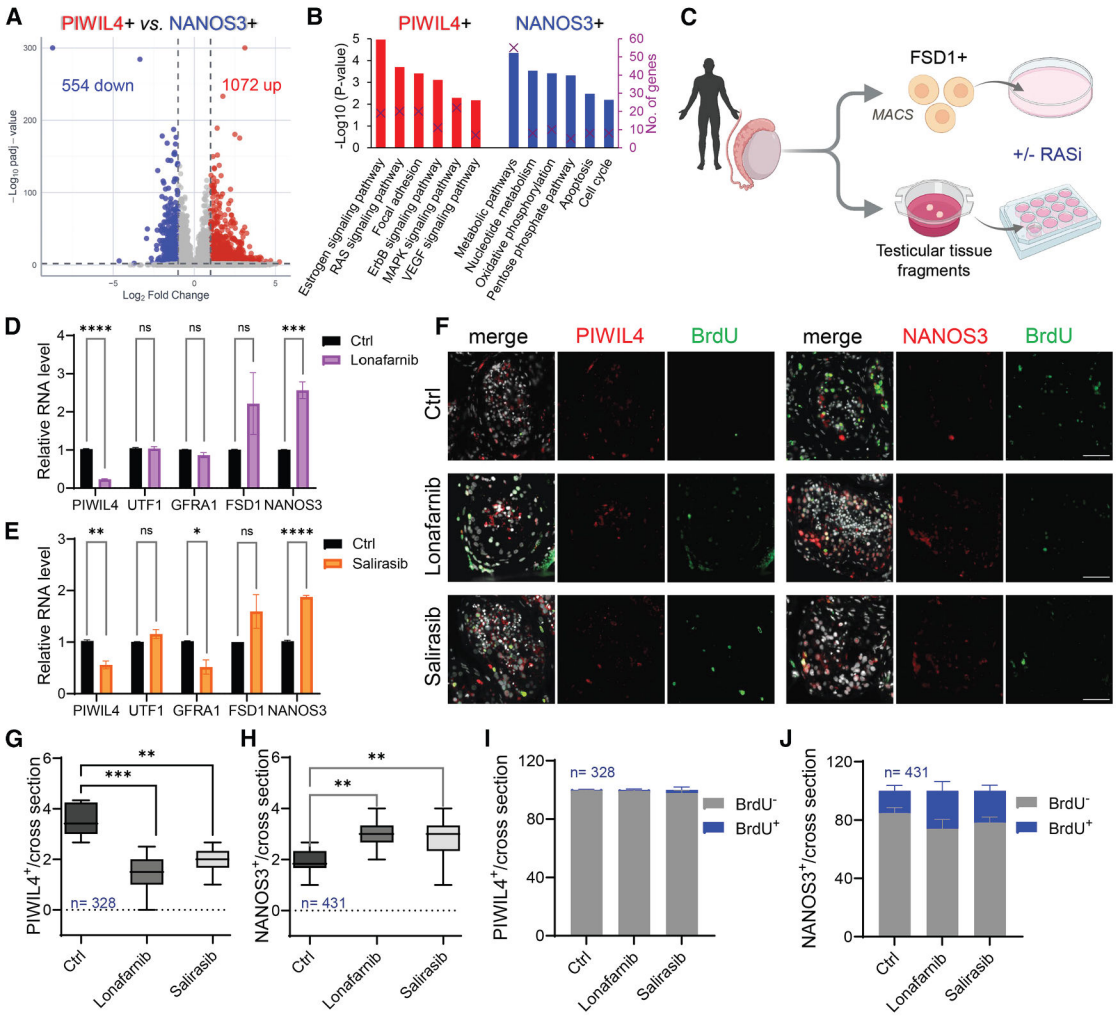

Figure 6. Evidence that the RAS signaling pathway promotes the uSPG primitive state

(A) Differentially expressed genes (DEGs; $q < 0.01$, fold change >2) from PIWIL4+ vs. NANOS3+ cells.

(B)Signaling pathways associated with the DEGs defined in (A). Statistical significance (−log10 (p value)) is indicated by the bar. The number of DEGs for a given category is indicated by an “X.”.

(C) Schematic of experimental design. Fresh human testis biopsies were processed in two ways: (1) dissociation followed by magnetic-activated cell sorting (MACS) to isolate FSD1+ uSPG for feeder-free culture with or without RAS inhibitors (RASis) or (2) maintained in transwell systems, also treated with or without RASis.

(D and E) RT-qPCR analysis of feeder-free human uSPG (enriched for FSD1+ cells) cultured for 1 week and treated with or without RASis: lonafarnib (D) and salirasib (E).

(F) Immunofluorescence analysis of human testicular tissue fragments cultured with or without RASis, stained for PIWIL4, NANOS3, and BrdU. Cell nuclei were counterstained with DAPI (gray). Scale bars: 50 μm.

(G and H) Quantification of PIWIL4+ ($n = 328$) and NANOS3+ ($n = 431$) per cross-section across four samples.

(I and J) BrdU index of PIWIL4+ (I) and NANOS3+ (J) cells in cultured testicular fragments, treated with or without RASis. Data are represented as the mean ± SEM. Four biological replications were performed.

For (D), (E), and (G)–(J), data are represented as the mean ± SEM. Four biological replications were performed. $^{**}p < 0.01$, $^{***}p < 0.001$, and $^{****}p < 0.0001$; ns, not statistically significant, as determined by unpaired *t* test (D and E) or one-way ANOVA (G–J).

KEY RESOURCES TABLE

REAGENT or RESOURCE	SOURCE	IDENTIFIER
Antibodies		
Rabbit polyclonal anti Human C19ORF81	Novus Biological	Cat# NBP2-32518; RRID:AB_3282455
Rabbit polyclonal anti Human C19ORF84	Atlas Antibodies	Cat# HPA068082; RRID:AB_2685949
Rabbit polyclonal anti Human CAMK2B	Novus Biologicals	Cat# NBP1-88212; RRID:AB_11016092
Rabbit polyclonal anti Human CCK	Novus Biologicals	Cat# NBP2-62664; RRID:AB_3353182
Mouse monoclonal anti Human CD82	Proteintech	Cat# 66803-1-Ig; RRID:AB_2882146
Rabbit polyclonal anti Human CDH15	Novus Biologicals	Cat# NBP1-88101; RRID:AB_11019082
Rabbit polyclonal anti Human CELF4	GeneTex	Cat# GTX121390; RRID:AB_11178502
Mouse monoclonal anti Human CELF4	DHSB	Cat# PCRP-CELF4-1C3; RRID:AB_2618496
Mouse monoclonal anti Human CTSG	MyBioSource	Cat# MBS555070; RRID:AB_3699235
Rabbit polyclonal anti Human CTSG	Boster Bio	Cat# PB10053; RRID:AB_3699237
Rabbit polyclonal anti Human EGR4	LifeSpan BioSciences	Cat# LS-C820482; RRID:AB_3699236
Rabbit polyclonal anti Human EGR4	LifeSpan BioSciences	Cat# LS-C402257; RRID:AB_2782963
Rabbit polyclonal anti Human ENO3	LifeSpan BioSciences	Cat# LS-C211358; RRID:AB_3699238
Mouse monoclonal anti Human FGFR3	Novus Biologicals	Cat# NBP2-52468; RRID:AB_2782964
Mouse monoclonal anti Human FGFR3	Thermo Fisher Scientific	Cat# MA5-26493; RRID:AB_2723178
Rabbit polyclonal anti Human FSD1	GeneTex	Cat# GTX131769; RRID:AB_2782962
Rabbit polyclonal anti Human GAL	Novus Biologicals	Cat# NBP2-33582; RRID:AB_3285153
Goat polyclonal anti Human GFRA1	R&D Systems	Cat# AF714; RRID:AB_355541
Rabbit polyclonal anti Human ITLN1	MyBioSource	Cat# MBS200265; RRID:AB_3699285
Rabbit polyclonal anti Human ITLN1	Proteintech	Cat# 11770-1-AP; RRID:AB_2129677
Rabbit polyclonal anti Human ITLN1	Elabscience	Cat# E-AB-68401; RRID: AB_3699286
Mouse monoclonal anti Human MKI67	Novus Biologicals	Cat# NBP2-22112; RRID:AB_3266743
Goat polyclonal anti Human KIT	R&D Systems	Cat# AF332; RRID:AB_355302
Mouse monoclonal anti Human NANOS2	LifeSpan BioSciences	Cat# LS-C73159-100; RRID:AB_1599930
Mouse monoclonal anti Human NANOS2	Santa Cruz Biotechnology	Cat# sc-393868; RRID:AB_3699234
Rabbit polyclonal anti Human NANOS3	Proteintech	Cat# 21679-1-AP; RRID:AB_1085925
Rabbit polyclonal anti Human NANOS3	Novus Biologicals	Cat# NBP1-76919; RRID:AB_11022652
Rabbit polyclonal anti Human PIWIL4	LifeSpan BioSciences	Cat# LS-C482396-50; RRID:AB_2782961
Rabbit polyclonal anti Human PLPPR3	Atlas Antibodies	Cat# HPA057034; RRID:AB_2683316
Mouse monoclonal anti Human PIWIL4	Novus Biologicals	Cat# NBP2-3739; RRID:AB_10859250
Mouse monoclonal anti Human PIWIL4	GeneTex	Cat# GTX60725; RRID:AB_3699239
Rabbit polyclonal anti Human PPP1R36	Novus Biologicals	Cat# NBP2-62718; RRID:AB_3353233
Rabbit polyclonal anti Human SH2B2	LifeSpan BioSciences	Cat# LS-C805414; RRID:AB_3699288
Rabbit polyclonal anti Human SOCS1	GeneTex	Cat# GTX100657; RRID:AB_1951971
Rabbit polyclonal anti Human TMEM181	Novus Biologicals	Cat# NBP1-93711; RRID:AB_1100592

REAGENT or RESOURCE	SOURCE	IDENTIFIER
Rabbit polyclonal anti Human TMEM181	Proteintech	Cat# 55411-1-AP; RRID:AB_11182284
Mouse monoclonal anti Human UCHL1	GeneTex	Cat# GTX34969; RRID:AB_3699240
Biological samples		
Testicular biopsies from 10 fertile men (Age 25–50 yrs)	UCSD	N/A
Testicular biopsies from 9 fertile men (aged 27, 28, 30, 34, 38, 38, 40, 40, and 46)	University of Pittsburgh Health Sciences Tissue Bank and Center for Organ Recovery	N/A
Chemicals, peptides, and recombinant proteins		
Human Recombinant bFGF	Thermo Fisher	Cat#NC1085507
Recombinant Human GDNF Protein	R&D Systems	Cat#212-GD
Lonafarnib (SCH66336)	Sellekchem	Cat#S2797
Salirasib	Sellekchem	Cat#S7684
Deposited data		
RNA sequencing data	This paper	GSE297876
Oligonucleotides		
See Table S3 for a list of primers	N/A	N/A
Software and algorithms		
STAR (v2.5.2b)	Dobin et al. 2013[51]	https://github.com/alexdobin/STAR
SubRead (featureCounts)	Liao et al. 2014[52]	http://subread.sourceforge.net
DESeq2	Love et al. 2014[53]	https://bioconductor.org/packages/release/bioc/html/DESeq2.html
pheatmap (R package)	Kolde 2025[54]	https://cran.r-project.org/web/packages/pheatmap/index.html
Metascape	Zhou et al. 2019[55]	https://metascape.org
Fiji (ImageJ)	Schindelin et al. 2012[56]	https://imagej.net/software/fiji/
SigmaPlot v14.0	Systat Software	https://systatsoftware.com/products/sigmaplot/
GraphPad Prism v9	GraphPad Software	https://www.graphpad.com/scientific-software/prism/
R v4.3.1	R Core Team	https://www.r-project.org